Materials Chemistry and Physics 153 (2015) 32–47

Contents lists available at ScienceDirect

Materials Chemistry and Physics

journal homepage: www.elsevier.com/locate/matchemphys

Thermodynamic modeling of Cu–Ni–Y system coupled with key experiments

Mohammad Mezbahul-Islam [a], Mamoun Medraj [a, b, *]

[a] Department of Mechanical Engineering, Concordia University, 1455 de Maisonneuve Blvd West, Montreal, Quebec, Montreal H3G 1M8, Canada
[b] Department of Mechanical and Materials Engineering, Masdar Institute of Science and Technology, Masdar City, Abu Dhabi, United Arab Emirates

HIGHLIGHTS

- Thermodynamic modeling of the Cu–Ni–Y system has been performed.
- Ternary solubilities of the binary compounds have been reproduced.
- Modified quasi-chemical model is used to model the liquid phase.
- DSC experiments are performed on selected key alloys.
- The calculations are consistent with the experimental results.

ARTICLE INFO

Article history:
Received 9 April 2014
Received in revised form
2 December 2014
Accepted 21 December 2014
Available online 6 January 2015

Keywords:
Phase equilibria
Phase transitions
Thermodynamic properties
Differential scanning calorimetry (DSC)
Electron microscopy

ABSTRACT

A complete thermodynamic description of the Cu–Ni–Y ternary system has been obtained using the CALPHAD (CALculation of PHAse Diagram) approach. Ternary solubility of the third element in the binary compounds in the Cu–Ni–Y system is described using sublattice model within the compound energy formalism (CEF) to take into account the recently reported experimental solubility ranges. The modified quasi-chemical model (*MQM*) has been used to describe the liquid phase in order to account for the presence of short range ordering properly. To study the melting behavior of the Cu–Ni–Y alloys and to verify the consistency of the thermodynamic model with experimental results, 10 key samples were prepared and the phase transformation temperatures were measured using differential scanning calorimeter (DSC). The microstructural characterization and crystallographic analysis of the alloys were carried out using scanning electron microscopy (SEM) coupled with WDS analysis and X-ray diffraction (XRD). Several vertical sections, liquidus projection and isothermal section at 973 K have been calculated and found to be in good agreement with the current experimental data as well as with the literature.

1. Introduction

The Cu–Ni–Y is one of the constituent ternaries of the Mg–Cu–Ni–Y quaternary system which is an important metallic glass system [1–5]. Magnesium-based bulk metallic glasses (BMG) have potential in many applications ranging from biomedical to sports equipment [6]. Also, rare earth (RE)-Ni based alloys are promising candidates for hydrogen storage and magnetic materials [7,8]. $Ni_{2.5}Cu_{0.5}Y$ was reported to have a promising hydrogen storage capacity [7]. $Ni_{17}Y_2$ was reported to have ferromagnetic characteristics when a small amount of Cu is added [8]. However, these applications especially the metallic glasses are very much composition dependant. Experimental determination of the best composition for any application of interest is time consuming and sometime is very difficult due to oxidation or reactivity of the elements. Hence, experiments alone are not always the most efficient technique. The use of thermodynamic calculations can significantly reduce the experimental efforts and time. A self-consistent thermodynamic database provides most of the vital information for developing new alloys. For instance, the impact of adding certain amount of Cu or Mg to $Ni_{2.5}Cu_{0.5}Y$ or any other composition with respect to temperature or pressure can be easily calculated. However, no thermodynamic description of the Cu–Ni–Y system could be found in the literature. Only two experimental works [9,10] were reported on the phase equilibria of this system. Therefore, the main objective of this work is to provide a sound thermodynamic description of the Cu–Ni–Y system using the current experimental

* Corresponding author. Department of Mechanical Engineering, Concordia University, 1455 de Maisonneuve Blvd West, Montreal, Quebec, Montreal H3G 1M8, Canada.
E-mail address: mmedraj@encs.concordia.ca (M. Medraj).

http://dx.doi.org/10.1016/j.matchemphys.2014.12.032
0254-0584/

results and all the available literature data.

In the present work, the optimized parameters of the constituent binaries: Ni–Y [11], Cu–Y [12] and Cu–Ni [13] are taken from the literature with small modification of the parameters of the intermetallic compounds due to the use of a different model. Most of the intermetallic compounds in the Ni–Y and Cu–Y systems exhibit ternary solubilities which have been described using sublattice modeling within the compound energy formulism (CEF). In the earlier assessments [11,12] these compounds were described using stoichiometric model. The liquid has been described using the modified quasichemical model (MQM) to consider the short range ordering. The liquidus of this system was not studied before. Hence differential scanning calorimetry (DSC) experiments have been performed on 10 key alloys in this work. The invariant reactions, the liquidus projection and the 973 K isothermal section of the Cu–Ni–Y system have been calculated using the obtained thermodynamic models. Besides, several vertical sections and phase assemblage diagrams are calculated and compared with the present experimental data.

2. Assessment of the literature data

The constituent binaries of the Cu–Ni–Y ternary system are Ni–Y, Cu–Y and Cu–Ni. All of these binaries have been previously thermodynamically modeled and their optimized parameters are available in the literature [11–13]. The most accurate thermodynamic description of the binary systems is used in the present work for the extrapolation to the ternary Cu–Ni–Y. A brief review of the literature is given below to summarize the status of these systems to date.

The phase diagram of the Ni–Y system was first investigated by Beaudry and Daane [14] and later by Domagala et al. [15]. Both studies showed similar features of the phase diagram except for one intermetallic compound, Ni_7Y_2. Domagala et al. [15] did not report the occurrence of Ni_7Y_2 which was found by Beaudry and Daane [14]. However, based on the crystallographic study of several Ni-RE (RE = rare earth) compounds by Buschow [16], Mezbahul-Islam and Medraj [11] accepted the presence of Ni_7Y_2 in the Ni–Y phase diagram. Several other assessments [17–20] on the Ni–Y phase diagram also considered this compound stable. Subramanian and Smith [18] determined the enthalpy of formation of the nine Ni–Y intermediate compounds using electromotive force (emf) measurements. Enthalpy of formation of these compounds was also estimated by [21–23]. Batalin et al. [24] measured the enthalpy of mixing of the liquid Ni–Y at 1973 K using differential thermal analysis (DTA). Considering the available experimental data, thermodynamic assessments were performed on the Ni–Y system by Nash [17], Du and Zhang [19], Mattern et al. [20] and Mezbahul-Islam and Medraj [11]. Ni–Y liquid showed high negative v-shaped experimental enthalpy of mixing [24] which is an indication of the presence of short range ordering (SRO). However, only Mezbahul-Islam and Medraj [11] considered SRO during thermodynamic modeling of the liquid. Therefore, in the present work, the optimized parameters reported by [11] will be used.

The Cu–Y system has five intermetallic compounds: Cu_6Y, Cu_4Y, Cu_7Y_2, Cu_2Y and CuY. Except Cu_6Y and Cu_7Y_2 all the compounds melt congruently. The Cu_6Y has a homogeneity range of, approximately, 13.0 ± 0.5 to 15.5 ± 0.5 at% Y at ~973 K [25]. Similar results were also reported by several other researchers [26–28]. Cu_4Y was also reported to have a homogeneity range by Chakrabarti and Laughlin [29] and Domagala et al. [15]. Nevertheless, the solubility of Cu_4Y could not be found in the investigations of Fries et al. [25] and Abend and Schaller [26]. Also, Okamoto [28] did not include any solubility for Cu_4Y in their assessment of the Cu–Y phase diagram. Accepting this, Mezbahul-Islam et al. [12] considered Cu_4Y stoichiometric in their thermodynamic optimization. Experimental investigation on the liquidus was carried out by [15,25–27,30]. The data of Domagala et al. [15] is associated with higher amount of error of ±15 K while for the others [25,26,30] the error is ~ ±5 K and are in close agreement. Measurements of the heat of mixing of liquid Cu–Y was carried out by [31–33] in the temperature range of 1300–1900 K. Activity of liquid Cu over the composition range 19.8–100 at% Cu at 1623 K was measured by Berezutskii and Lukashenko [34] and that of liquid Y was reported by Abend and Schaller [26]. In addition, Enthalpy of formation of the compounds was determined by Watanabe and Kleppa [33]. Thermodynamic modeling of the Cu–Y system has been performed by Fries et al. [25], Abend and Schaller [26], Boudene et al. [35], Itagaki et al. [36] and more recently by Mezbahul-Islam et al. [12]. In the present work, the optimized parameters of the Cu–Y binary reported by Mezbahul-Islam et al. [12] are used for the evaluation of the Cu–Ni–Y ternary, because these authors [12] considered all the available information from the literature during optimization and reproduced the phase diagram and thermodynamic properties within the experimental error limits. Also, they used *MQM* model to describe the liquid phase that showed short range ordering at approximately 30 at% Y.

Cu–Ni is a very well-known isomorphous system. The liquid phase is miscible in all proportions. The fcc(Cu, Ni) solid solution is also miscible down to the critical (T_c) temperature where it shows immiscibility for a wide range. This phase shows magnetic property at lower temperature (>~500 K). A complete assessment of this system was done by Hansen and Anderko [37] and later by Chakrabarti and Laughlin [38]. Recent studies on the phase equilibria of the Cu–Ni system were done by [39–41] using XRD and microstructural analysis. The presence of the immiscibility in the fcc(Cu,Ni) phase is an important issue in this system. Several studies [42–45] on the electric, magnetic and structural properties of the alloys and their low temperature heat capacity confirmed the existence of this immiscibility. Also large number of studies on the thermodynamic properties on the liquid and solid phases could be found in the literature [41,46–61]. Thermodynamic modeling of this system was done by Mey [62], Turchanin et al. [63] and Mezbahul-Islam and Medraj [13]. Both Mey [62] and Turchanin et al. [63] modeled the system quite well using Bragg-Williams model which is suitable for random mixing solutions and Cu–Ni system does not show any indications of short range ordering in the liquid. However, the other two binary systems show short range ordering which can be thermodynamically described better using the *MQM* model. Therefore, in order to be compatible with Cu–Y and Ni–Y systems, the optimized parameters of the Cu–Ni system reported by Mezbahul-Islam and Medraj [13] will be used in the present work.

The calculated Ni–Y, Cu–Y and Cu–Ni binary phase diagrams along with the available experimental data from the literature are shown in Fig. 1(a–c).

The Cu–Ni–Y ternary system was investigated by Zheng and Nong [9] who reported a partial isothermal section ($Y \leq 16.7$ at%) at room temperature based on XRD. They reported two three-phase equilibrium regions among Cu_6Y, Ni_5Y and fcc(Cu,Ni) phases and Ni_5Y, $Ni_{17}Y_2$ and fcc(Cu,Ni) phases. They also reported the solubility of Cu in $Ni_{17}Y_2$ to be about 35 at% and the maximum solubility of Y in the fcc(Cu,Ni) phase to be less than 1.5 at%. Crystallographic analysis of the Cu–Ni–Y alloys were performed by a few research groups [64–66] for different applications. Kadomatsu and Kurisu [64] studied the structural phase transitions in $Cu_{1-x}Ni_xY$ alloys and reported that the CsCl type CuY phase changes to FeB type structure at low temperature. Based on this analysis, Gupta [67] predicted a complete mutual solubility between CuY and NiY since NiY also has a FeB type crystal structure. Later, Mezbahul-Islam and Medraj [10]

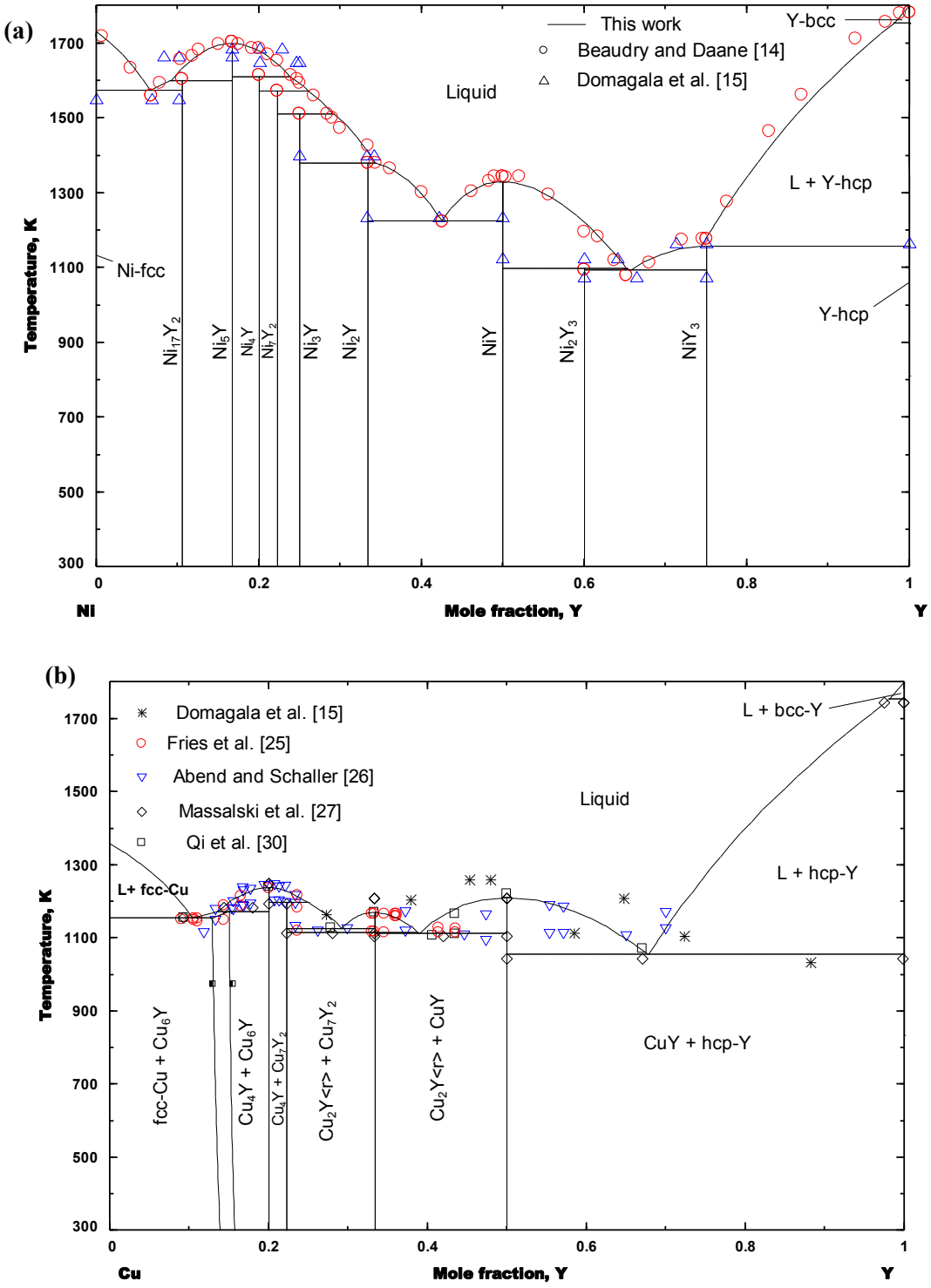

Fig. 1. Calculated binary phase diagrams: (a) Ni–Y; (b) Cu–Y; (c) Cu–Ni.

proved the complete solubility of CuY–NiY using XRD and EPMA analysis of many key alloys. Paul-Boncour et al. [65] studied the $(Ni,Cu)_2Y$ pseudobinary compounds for the structural change of the cubic Ni_2Y phase to the orthorhombic Cu_2Y phase using XRD, neutron diffraction, density measurement and electron microprobe analysis. According to their assessment, the maximum solubility of Ni and Cu in Cu_2Y and Ni_2Y are ~30.5 and 10.4 at% respectively, at 1023 K. Dwight [66] studied the crystal structures of several $Cu_xNi_{5-x}Y$ alloys to understand the solubility of Cu in the Ni_5Y compound by XRD. According to their report, Ni_5Y has a solubility of about 66.67 at% Cu at 1073 K. Burnasheva and Tarasov [7] studied the hydrogen storage capacity of Ni_3Y by partially replacing Ni with other transition elements. They found Ni_3Y to be stable untill 12.50 at% Cu at 770 K.

The latest experimental assessment on the Cu–Ni–Y system has been provided by Mezbahul-Islam and Medraj [10]. They

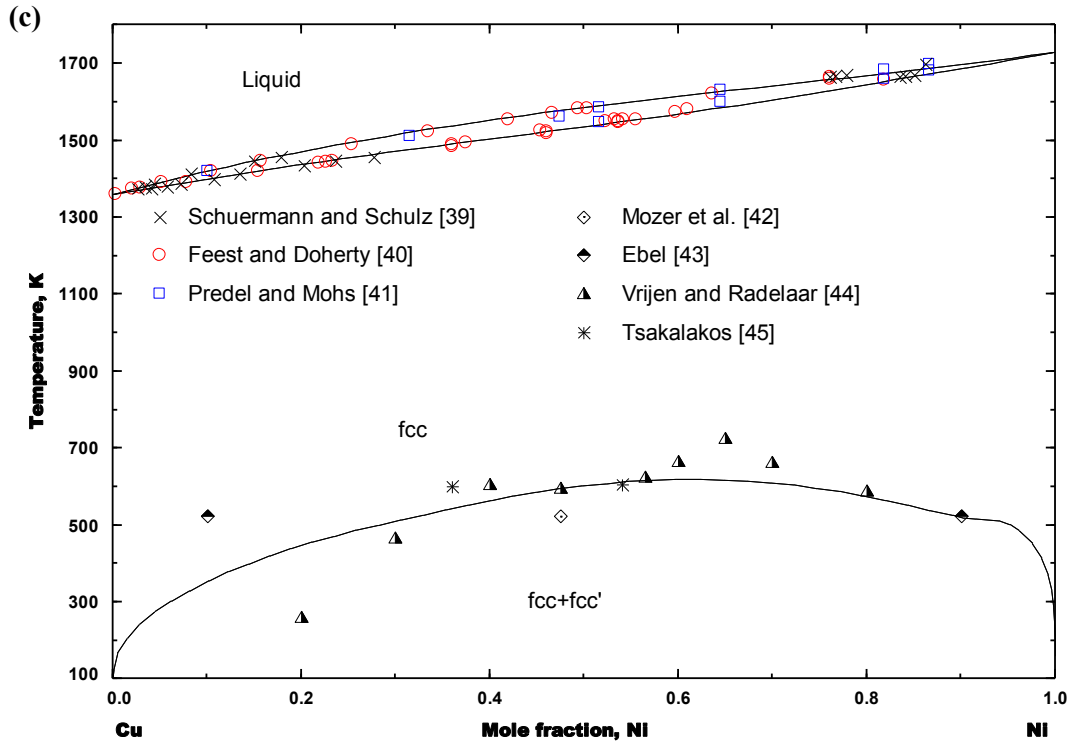

Fig. 1. (*continued*).

investigated this system using solid–solid diffusion couples and key sample analysis and provided an isothermal section for the whole composition range at 973 K. The main feature of their assessment is the determination of two complete mutual solubility between CuY–NiY and Cu_4Y–Ni_4Y. These two phases will be represented as (Cu,Ni)Y and $(Cu,Ni)_4Y$ through out the paper. The maximum ternary solubility of the intermetallic compounds in the Cu–Y and Ni–Y systems was also reported by [10]. The maximum solubility of Ni in Cu_2Y and Cu_7Y_2 was found to be ~28 and 3.6 at% Ni, respectively. The solubility of Cu in NiY_3, Ni_2Y, Ni_3Y, Ni_7Y_2, Ni_5Y and $Ni_{17}Y_2$ is about 12.0, 9.7, 25.0, 3.1, 75.0 and 37.0 at%. Cu, respectively. In addition 2 single-phase region, 21 two-phase regions and 10 three-phase regions are reported in [10]. The phase relations of the Cu–Ni–Y system provided by Mezbahul-Islam and Medraj [10] are qualitatively in agreement with that of Zheng and Nong [9] (Y ≤ 16.7 at%) and with the assessment of Gupta [67].

In the present paper, the latest understanding of the phase relationships provided by Mezbahul-Islam and Medraj [10] along with the current new experimental results are used to model the Cu–Ni–Y system. Also, all the experimental data from literature [9,65–67] will be compared with the current thermodynamic modeling.

3. Thermodynamic models

3.1. Pure elements

The Gibbs energy of pure element i (i = Cu, Ni, Y) in a certain phase ϕ is described as a function of temperature by the following equation:

$$^{0}G_i^{\phi}(T) = a + bT + cTlnT + dT^2 + eT^3 - fT^{-1} + gT^7 + hT^{-9} \quad (1)$$

where, $^{0}G_i^{\phi}$ is the Gibbs energy at the standard state and T is the absolute temperature. The values of the coefficients a to h are taken from the SGTE (Scientific Group Thermodata Europe) compilation by Dinsdale [68].

3.2. Intermediate stoichiometric compounds

Gibbs energy of the stoichiometric compounds is described using the following expression:

$$G^{\varphi} = x_i^0 G_i^{\varphi} + x_j^0 G_j^{\varphi} + x_k^0 G_k^{\varphi} + \Delta G^f \quad (2)$$

where, φ denotes the phase of interest, x_i, x_j and x_k are the mole fraction of components i, j and k and G_i^{φ}, G_j^{φ} and G_k^{φ} represent the Gibbs energy of the components, i, j and k, in their standard state. $\Delta G^f (=a + bT)$ represents the Gibbs energy of formation of 1 mol of the stoichiometric compound. The parameters, a and b are determined considering the experimental data (enthalpy and entropy of formation, melting temperature etc.) of the compounds. In the present work, Ni_2Y_3 in the Ni–Y system and Cu_2Y(h) in the Cu–Y system have been modeled using the stoichiometric model as reported by [11,12]. The Cu–Ni–Y system does not have any ternary stoichiometric compound.

3.3. Terminal solid solution

The fcc^{Cu-Ni}, fcc^{Ni-Y}, fcc^{Cu-Y}, hcp-Y^{Cu-Y}, and hcp-Y^{Ni-Y} terminal solid solutions are modeled using the Bragg-Williams (B–W) model. Unlike the liquid phase, short range ordering was not found in the terminal solid solutions of the constituent binaries of the Cu–Ni–Y system. Hence, random solution (B–W) model is used for the modeling. The Gibbs energy of these phases can be expressed as:

$$G = x_i^0 G_i^\varphi + x_j^0 G_j^\varphi + RT\left[x_i lnx_i + x_j lnx_j\right] + {}^{ex}G^\varphi + {}^{ex}G_{mag}^\varphi \quad (3)$$

where, ${}^{ex}G^\varphi$ is the excess Gibbs energy function which is expressed using the Redlich-Kister polynomial:

$${}^{ex}G^\varphi = X_A X_B\left[{}^0L_{A,B}^\varphi + (X_A - X_B)^1 L_{A,B}^\varphi + (X_A - X_B)^{22} L_{A,B}^\varphi\right] \quad (4)$$

Each of the L terms may be temperature dependent according to

$${}^nL_{A,B}^\varphi = a + bT \quad (5)$$

The parameters a and b are obtained by optimization using experimental results of phase equilibria and thermodynamic data. The last term, ${}^{ex}G_{mag}^\varphi$, in equation (3), is the magnetic contribution to the Gibbs energy. The Cu–Ni alloys showed magnetic susceptibility. Therefore, ${}^{ex}G_{mag}^\varphi$ has been used to describe the magnetic contribution for the fcc (Cu,Ni) phase. Explanation of the magnetic contribution to the fcc (Cu,Ni) phase has been discussed earlier [13].

3.4. Intermediate solid solution phases

In order to represent the ternary solubility of the binary compounds: (Cu,Ni)Y, $(Cu,Ni)_4Y$, Cu_2Y(r), Cu_7Y_2, Cu_6Y, NiY_3, Ni_2Y, Ni_3Y, Ni_5Y and $Ni_{17}Y_2$, in the Cu–Ni–Y system, sublattice model has been used. The number of sublattice is determined based on the crystallographic information of the compounds. The Gibbs energy of these compounds can be represented using the compound energy formalism (CEF) as:

$$G = G^{ref} + G^{ideal} + G^{excess} \quad (6)$$

$$G^{\text{ref}} = \sum y_i^l y_j^m \ldots y_k^q {}^oG_{(i:j:\ldots:K)} \quad (7)$$

$$G^{\text{ideal}} = \text{RT}\sum_l f_l \sum_l y_i^l lny_i^l \quad (8)$$

$$G^{\text{excess}} = \sum y_i^l y_j^l y_k^m \sum_{\gamma=0}^{\gamma} {}^\gamma L_{(i,j):k} \times \left(y_i^l - y_j^l\right)^\gamma \quad (9)$$

where, i, j, … k represent components or vacancy in l, m and q sublattices. y_i^l represents the site fraction of component i on sublattice l; f_l is the fraction of sublattice l relative to the total lattice sites, ${}^oG_{(i,j,\ldots,k)}$ represents the compound energy of a real or a hypothetical end member in the sublattice model. ${}^\gamma L_{(i,j):k}$ represents the interaction parameters which describe the interaction between the constituents within the sublattice.

3.5. Liquid phase

The modified quasichemical model (*MQM*) [69–72] in the pair approximation was used to describe the thermodynamic properties of the liquid solution in this work. Both Ni–Y and Cu–Y liquid have very high negative V-shaped asymetric enthalpy of mixing [11,12]. This is an indication of the occurrence of short range ordering in the liquid phase [73]. Therefore to treat short-range ordering effectively, the *MQM* in the pair approximation has been used in the present study. Since the *MQM* Model can give more realistic thermodynamic description for liquid solutions than the conventional random-mixing Bragg Williams model. This model (*MQM*) has three distinct characteristics: It permits choosing the composition of maximum short range ordering in a binary system. It expresses the energy of pair formation as a function of composition which can be expanded as a polynomial in the pair fraction. The model can be extended to multicomponent system [69].

To elaborate on this model, the following pair exchange reaction in a hypothetical A–B system can be discussed

$$(A-A)_{pair} + (B-B)_{pair} = 2(A-B)_{pair}; \Delta g_{AB} \quad (10)$$

In equation (10), $(i\text{-}j)_{pair}$ represents the first-nearest-neighbor pair and Δg_{AB} is the non-configurational Gibbs energy change for the formation of 2 mol of $(i\text{-}j)_{pair}$ [69–72]. The Gibbs energy of the binary A–B solution can be written as:

$$G = \left(n_A g_A^o + n_B g_B^o\right) - T\Delta S^{config} + \left(\frac{n_{AB}}{2}\right)\Delta g_{AB} \quad (11)$$

here, g_A^o and g_B^o are the molar Gibbs energies of the pure liquid, n_A and n_B are the number of moles of the components A and B, n_{AB} is the number of $(A–B)$ pairs, ΔS^{config} is the configurational entropy of mixing given by random distribution of $(A–A)$, $(B–B)$ and $(A–B)$ pairs which can be expressed as equation (12):

$$\Delta S^{config} = -R(n_A lnx_A + n_B lnx_B) - R\left[n_{AA}\ln\left(\frac{X_{AA}}{Y_A^2}\right) + n_{BB}\ln\left(\frac{X_{BB}}{Y_B^2}\right) + n_{AB}\ln\left(\frac{X_{AB}}{2Y_A Y_B}\right)\right] \quad (12)$$

where, x_A and x_B are the overall mole fractions of A and B. n_{AA} and n_{BB} are the number of $(A–A)$ and $(B–B)$ pairs. X_{AA}, X_{BB} and X_{AB} are the pair fractions and can be expressed as in equation (13):

$$X_{AA} = \frac{n_{AA}}{n_{AA}+n_{BB}+n_{AB}}; X_{BB} = \frac{n_{BB}}{n_{AA}+n_{BB}+n_{AB}}; X_{AB} = \frac{n_{AB}}{n_{AA}+n_{BB}+n_{AB}} \quad (13)$$

Y_A and Y_B in equation (12) are the coordination equivalent fraction and can be expressed as in equation (14):

$$Y_A = \frac{Z_A n_A}{Z_A n_A + Z_B n_B} = \frac{Z_A X_A}{Z_A X_A + Z_B X_B} = 1 - Y_B \quad (14)$$

where, Z_A and Z_B are the coordination numbers of A and B which can be represented by equations (15) and (16).

$$\frac{1}{Z_A} = \frac{1}{Z_{AA}^A}\left(\frac{2n_{AA}}{2n_{AA}+n_{AB}}\right) + \frac{1}{Z_{AB}^A}\left(\frac{n_{AB}}{2n_{AA}+n_{AB}}\right) \quad (15)$$

$$\frac{1}{Z_B} = \frac{1}{Z_{BB}^B}\left(\frac{2n_{BB}}{2n_{BB}+n_{AB}}\right) + \frac{1}{Z_{BA}^B}\left(\frac{n_{AB}}{2n_{BB}+n_{AB}}\right) \quad (16)$$

Table 1
Optimized *MQM* model parameters for the liquid phase in the Cu–Ni–Y system.

System	Parameters
	Unit for Gibbs energy terms (Δg) (J/mole); coordination number (Z) is dimensionless.
Cu–Ni	$Z_{CuNi}^{Cu} = 6$, $Z_{NiCu}^{Ni} = 6$ $\Delta g_{CuNi}^0 = 5797.3 - 0.21T$; $\Delta g_{CuNi}^{10} = -1172.02$
Cu–Y	$Z_{CuY}^{Cu} = 3$, $Z_{YCu}^{Y} = 6$ $\Delta g_{CuY}^0 = -28718.77 + 6.28T$; $\Delta g_{CuY}^{10} = -6446.13 + 0.84T$; $\Delta g_{CuY}^{01} -6906.57 + 2.09T$
Ni–Y	$Z_{NiY}^{Ni} = 5$, $Z_{YNi}^{Y} = 6$ $\Delta g_{NiY}^0 = -33\,653.83 + 1.61T$; $\Delta g_{NiY}^{01} = -1339.46 + 1.26T$; $\Delta g_{NiY}^{10} = -17\,538.50$
Cu–Ni–Y	$g_{CuY(Ni)}^{001} = 1674.32$; $g_{NiY(Cu)}^{001} = -2092.90$

Table 2
Optimized model parameters for the terminal and intermediate solid solutions in the Cu–Ni–Y system. Reference state of the pure solids used for creation of the end members: Cu (fcc), Ni (fcc) and Y (hcp).

Phase	Model used	Parameters
		Unit for T is K, G is J/mole; H is J/mole; S is J/mole.K, Cp is J/K, $^{0}T_c$ is K, $^{0}\beta$ is Bohr-magneton
fcc	B–W	${}^{o}L^{fcc}_{Cu,Ni} = 6\,793.40 + 4.65\,T$; ${}^{1}L^{fcc}_{Cu,Ni} = 1\,655.80$;
		${}^{o}L^{fcc}_{Ni,Y} = 3\,675.18$
		${}^{o}L^{fcc}_{Cu,Y} = 41\,858.00$
		${}^{o}T^{fcc}_{c(cu,Ni)} = -467.5$; ${}^{1}T^{fcc}_{c(Cu,Ni)} = -297.5$;
		${}^{o}\beta^{fcc}_{CuNi} = -0.7316$; ${}^{o}\beta^{fcc}_{CuNi} = -0.3170$
Y-hcp	B–W	${}^{o}L^{hcp}_{Cu,Y} = 40\,221.35$
		${}^{o}L^{hcp}_{Cu,Ni} = 10\,004.30$
Y-bcc	B–W	${}^{o}L^{Y-bcc}_{Ni,Y} = 62\,787.00$
Ni_2Y_3	Stoichiometric	$\Delta H^{0}_{298.15} = -143700$; $S^{0}_{298.15} = 193.3089$
		$C_p = 2^{*}\,C_p$ (Ni-fcc) + $3^{*}\,C_p$ (Y-hcp)
Cu_2Y(h)	Stoichiometric	$\Delta H^{0}_{298.15} = -52248.458$; $S^{0}_{298.15} = 115.60948$
		$C_p = 2^{*}\,C_p$ (Cu-fcc) + C_p (Y-hcp)
(Cu,Ni)Y (Y%) (Cu, Ni)	Sub-lattice	${}^{o}G^{(Cu,Ni)Y}_{Y:Cu} = -42\,124.40 + 3.98T$;
		${}^{o}G^{(Cu,Ni)Y}_{Y:Ni} = -70\,569.07 + 1.67T$
		${}^{o}L^{(Cu,Ni)Y}_{Y:Cu,Ni} = -10\,464.50 + 11.72T$
$(Cu, Ni)_4Y$ (Y%) $(Cu, Ni)_4$	Sub-lattice	${}^{o}G^{(Cu,Ni)_4Y}_{Y:Cu} = -89\,479.85 + 8.25T$;
		${}^{o}G^{(Cu,Ni)_4Y}_{Y:Ni} = -156\,260.52 + 8.25T$
		${}^{o}L^{(Cu,Ni)_4Y}_{Y:Cu,Ni} = -52\,113.21 + 66.14T$
Cu_2Y (R) (Y%) (Cu%, Ni)$_2$	Sub-lattice	${}^{o}G^{Cu_2Y}_{Y:Cu} = -65\,997.09 + 7.42T$;
		${}^{o}G^{Cu_2Y}_{Y:Ni} = -83\,393.69 + 5.27T$;
		${}^{o}L^{Cu_2Y}_{Y:Cu,Ni} = -104\,226.42 + 60.69T$
Cu_7Y_2 (Y%)$_2$ (Cu%, Ni)$_7$	Sub-lattice	${}^{o}G^{Cu_7Y_2}_{Y:Cu} = -168\,977.40 + 15.58T$
		${}^{o}G^{Cu_7Y_2}_{Y:Ni} = -269\,380.51 + 11.82T$;
		${}^{o}L^{Cu_7Y_2}_{Y:Cu,Ni} = -62\,787.0 + 85.81T$
Cu_6Y (Cu%)$_5$ (Y%, Cu_2, Ni)	Sub-lattice	${}^{o}G^{Cu_6Y}_{Cu:Y} = -21\,500.00 + 8.37T$; ${}^{o}G^{Cu_6Y}_{Cu:Cu_2} = 9\,700.59 + 6.91T$;
		${}^{o}G^{Cu_6Y}_{Cu:Ni} = {}^{o}G^{Cu_6Y}_{Ni:Cu_2}\,16\,743.20$; ${}^{o}G^{Cu_6Y}_{Ni:Y} = 8\,371.6$;
		${}^{o}G^{Cu_6Y}_{Ni:Ni} = 33\,486.40$;
		${}^{o}L^{Cu_6Y}_{Cu,Y:Cu_2} = -11\,797.70 + 7.08T$;
		${}^{o}L^{Cu_6Y}_{Ni:Y,Cu_2} = -146\,503.0 + 117.20T$;
		${}^{o}L^{Cu_6Y}_{Cu,Ni:Y} = -230\,219.0 + 87.90T$
NiY_3 (Y%)$_3$ (Ni%, Cu)	Sub-lattice	${}^{o}G^{NiY_3}_{Y:Ni} = -76\,878.08 + 1.75T$;
		${}^{o}G^{NiY_3}_{Y:Cu} = -39\,346.52 + 14.65T$;
		${}^{o}L^{NiY_3}_{Y:Ni,Cu} = -33\,486.40 + 12.56T$
Ni_2Y (Y%) (Ni%, Cu)$_2$	Sub-lattice	${}^{o}G^{Ni_2Y}_{Y:Ni} = -112\,168.10 + 6.11T$;
		${}^{o}G^{Ni_2Y}_{Y:Cu} = -23\,737.67 + 7.42T$;
		${}^{o}L^{Ni_2Y}_{Y:Ni,Cu} = -66\,554.22 + 30.56T$
Ni_3Y (Y%) (Ni%, Cu)$_3$	Sub-lattice	${}^{o}G^{Ni_3Y}_{Y:Ni} = -134\,388.04 + 4.77T$; ${}^{o}G^{Ni_3Y}_{Y:Cu} = -15\,989.76 + 6.28T$;
		${}^{o}L^{Ni_3Y}_{Y:Ni,Cu} = -118\,248.85 + 45.63T$
Ni_7Y_2 (Y%)$_2$ (Ni%, Cu)$_7$	Sub-lattice	${}^{o}G^{Ni_7Y_2}_{Y:Cu} = -127\,172.97 + 15.58T$
		${}^{o}G^{Ni_7Y_2}_{Y:Ni} = -290\,309.51 + 11.82T$;
		${}^{o}L^{Ni_7Y_2}_{Y:Ni,Cu} = -62\,787.0 + 56.51T$
Ni_5Y (Y%) (Ni%, Cu)$_5$	Sub-lattice	${}^{o}G^{Ni_5Y}_{Y:Ni} = -170\,100.96 + 9.15T$; ${}^{o}G^{Ni_5Y}_{Y:Cu} = -87\,828.05 + 6.86T$;
		${}^{o}L^{Ni_5Y}_{Y:Ni,Cu} = -77\,018.72 + 89.99T$
$Ni_{17}Y_2$ (Ni%, Cu)$_{12}$ (Ni%,Cu)$_3$ (Ni%, Cu)$_2$ (Y%)$_2$	Sub-lattice	${}^{o}G^{Ni_{17}Y_2}_{Ni:Ni:Ni:Y} = -374\,546.82 + 33.83T$
		${}^{o}G^{Ni_{17}Y_2}_{Ni:Ni:Cu:Y} = -376\,722.0 + 41.86T$;
		${}^{o}G^{Ni_{17}Y_2}_{Ni:Cu:Ni:Y} = -418\,580.0 + 80.36T$;
		${}^{o}G^{Ni_{17}Y_2}_{Ni:Cu:Cu:Y} = {}^{o}G^{Ni_{17}Y_2}_{Cu:Ni:Ni:Y} = {}^{o}G^{Ni_{17}Y_2}_{Cu:Ni:Cu:Y} = 5000.0$;
		${}^{o}G^{Ni_{17}Y_2}_{Cu:Cu:Ni:Y} = -246\,962.20 + 79.53T$;
		${}^{o}G^{Ni_{17}Y_2}_{Cu:Cu:Cu:Y} = -125\,574.0 + 100.46T$;
		${}^{o}L^{Ni_{17}Y_2}_{Ni,Cu:Ni:Ni:Y} = -226\,033.20 + 104.65T$;
		${}^{1}L^{Ni_{17}Y_2}_{Ni,Cu:Ni:Ni:Y} = 39\,346.52$;
		${}^{o}L^{Ni_{17}Y_2}_{Ni,Cu:Ni,Cu:Ni:Y} = -385\,093.60 + 125.57T$

Z^A_{AA} and Z^A_{AB} are the values of Z_A when all nearest neighbors of an A atom are A's, and when all nearest neighbors of A atom are B's, respectively. Similarly for Z^B_{BB} and Z^B_{BA}. Z^A_{AA} and Z^B_{BB} are defined similarly and it has been found that number in the order of 6 is necessary for a solution with small or medium degree of *SRO* [11,74–79]. The composition of maximum short range ordering is determined by the ratio Z^B_{BA}/Z^A_{AB} [69–72]. Values of Z^A_{AB} and Z^B_{BA} are unique to the A–B binary system and should be carefully determined to fit the thermodynamic experimental data (enthalpy of mixing, activity etc.). The *MQM* model is sensitive to the ratio of coordination numbers, but less sensitive to their absolute values. The coordination numbers used in this work are listed in Table 1 for the different binary systems.

The energy of pair formation Δg_{AB} in equation (11), is the model parameter to reproduce the Gibbs energy of liquid phase of the binary system, which can be expressed as a polynomial in terms of the pair fraction as shown in equation (17) [69].

$$\Delta g_{AB} = \Delta g^o_{AB} + \sum_{i\geq 1} g^{io}_{AB} X^i_{AA} + \sum_{j\geq 1} g^{oj}_{AB} X^j_{BB} \tag{17}$$

where, Δg^o_{AB}, g^{io}_{AB} and g^{oj}_{AB} are the model parameters and can be expressed as functions of temperature. These binary liquid parameters are adopted from our previous works on Mg–Cu–Y [12], Mg–Ni–Y [11] and Mg–Cu–Ni [13] systems.

The thermodynamic properties of the ternary liquid were extrapolated using an asymmetric 'Toop like' approximation [80]. According to Qiao et al. [81], if the excess thermodynamic properties in two of the three binary systems show similarity and significantly differ from the third one, the ternary system should be considered as an asymmetric system and the common component in the two similar binary systems should be chosen as the asymmetric component. The Gibbs energy of the Cu–Y [12] and Ni–Y [11] liquid have strong negative deviation whereas Cu-Ni [13] has positive deviation from ideal solution. Hence, yttrium has been singled out as the asymmetric component during the extrapolation.

Table 3
Ternary solubility of the Cu–Y and Ni–Y compounds in the Cu–Ni–Y ternary system.

Phase	Ternary solubility calculated (this work)	Ternary solubility measured (literature)	Temperature of measurement
Cu_2Y	26.5 at% Ni	28.0 at% Ni [10].	973 K
		30.5 at% Ni [65].	923–1123 K
Cu_7Y_2	3.2 at% Ni	~3.6 at% Ni [10].	973 K
Cu_6Y	5.1 at% Ni	~5.0 at% Ni [9].	300 K
NiY_3	10.3 at% Cu	12.0 at% Cu [10].	973 K
Ni_2Y	9.9 at% Cu	9.7 at% Cu [10].	973 K
		10.4 at% Cu [65].	923–1123 K
Ni_3Y	18.7 at% Cu	25.0 at% Cu [10].	973 K
		≥12.50 at% Cu [7].	≤470 K
Ni_7Y_2	1.5 at% Cu	3.1 at% Cu [10].	973 K
Ni_5Y	74.4 at% Cu	75.0 at% Cu [10].	973 K
		≥66.67 at% Cu [66].	1073 K
		Complete solubility with Cu [9].	300 K
$Ni_{17}Y_2$	33.0 at% Cu	37.0 at% Cu [10].	973 K
		35 at% Cu [9].	300 K

Therefore, the Gibbs energy of the binary Cu–Y, Ni–Y and Cu–Y have been extrapolated to the ternary Cu–Ni–Y system by the extended Modified Quasichemical Model as described by Pelton and Chartrand [70] for the multicomponent asymmetric system according to the following equations:

$$\Delta g_{CuY} = \left(\Delta g^o_{CuY} + \sum_{(i+j)\geq 1} g^{ij}_{CuY}(1-Y_{Cu})^j\right) + \sum_{\substack{k\geq 1\\ i\geq 0\\ j\geq 0}} g^{ijk}_{CuY(Ni)} Y^i_{Cu}(1-Y_{Cu})^j \left(\frac{Y_{Ni}}{Y_Y + Y_{Ni}}\right)^k \tag{18}$$

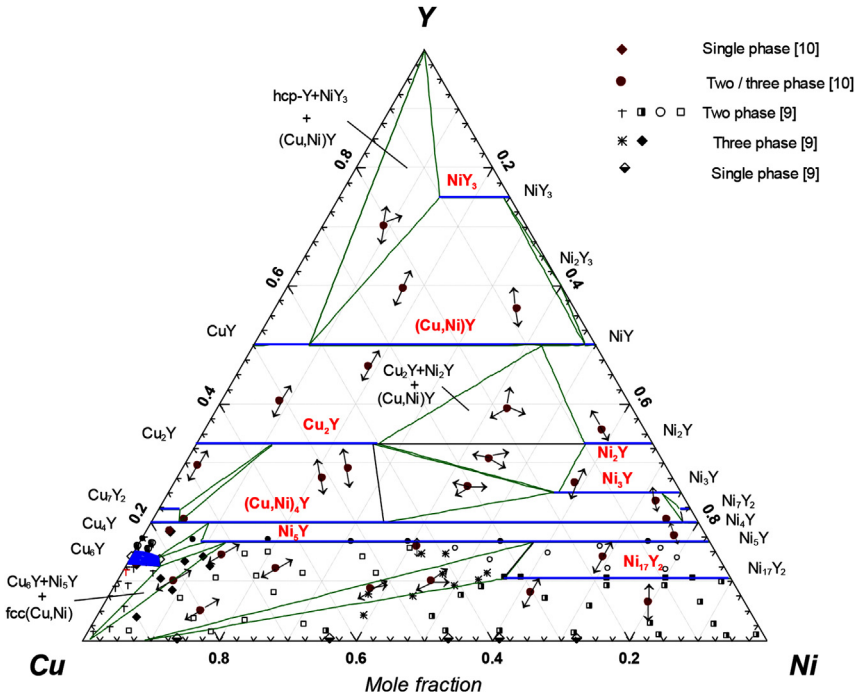

Fig. 2. Calculated isothermal section of the Cu–Ni–Y system at 973 K.

$$\Delta g_{NiY} = \left(\Delta g^{o}_{NiY} + \sum_{(i+j)\geq 1} g^{ij}_{NiY}(1-Y_{Ni})^{j}\right) + \sum_{\substack{k\geq 1\\ i\geq 0\\ j\geq 0}} g^{ijk}_{NiY(Cu)} Y^{i}_{Ni}(1-Y_{Ni})^{j}\left(\frac{Y_{Cu}}{Y_{Y}+Y_{Cu}}\right)^{k} \quad (19)$$

$$\Delta g_{CuNi} = \left(\Delta g^{o}_{CuNi} + \sum_{(i+j)\geq 1} g^{ij}_{CuNi}\left(\frac{Y_{Cu}}{Y_{Cu}+Y_{Ni}}\right)^{i}\left(\frac{Y_{Ni}}{Y_{Cu}+Y_{Ni}}\right)^{j}\right) + \sum_{\substack{k\geq 1\\ i\geq 0\\ j\geq 0}} g^{ijk}_{CuNi(Y)}\left(\frac{Y_{Cu}}{Y_{Cu}+Y_{Ni}}\right)^{i}\left(\frac{Y_{Ni}}{Y_{Cu}+Y_{Ni}}\right)^{j} Y^{k}_{Y} \quad (20)$$

where $g^{ijk}_{CuY(Ni)}$, $g^{ijk}_{NiY(Cu)}$ and $g^{ijk}_{CuNi(Y)}$ are the ternary interaction parameters which need to be determined to be consistent with the experimental data.

4. Experimental procedure

To investigate the liquidus of the Cu–Ni–Y system and to confirm the consistency of the thermodynamic model with experimental results, 10 key samples were analyzed. The purity of the elements used is Cu-99.99%, Ni-99.99%, and Y-99.9%, all supplied by Alfa Aesar. The alloys were prepared in an arc-melting furnace with water-cooled copper crucible in an argon atmosphere using a non-consumable tungsten electrode. Each alloy was crushed and re-melted at least four times to ensure homogeneity. The actual global composition of the samples was determined by Inductively Coupled Plasma (Ultima 2 ICP–OES) spectrometer. The melting and phase transformations temperatures were obtained using 5 and 10 K/min heating and cooling rates by means of a SETARAM differential scanning calorimeter (DSC) under a continuous flow of argon. Temperature calibration of the DSC was done using standard samples of Sn, Al, Zn, Ni, Ag and Au. Samples were placed in an alumina (Al_2O_3) crucible covered with a lid. The reproducibility of every measurement was confirmed by collecting the data during three different heating and cooling cycles for each sample. The estimated error of measurements between the repetitive cycles is ±5 K or less. Temperatures corresponding to various thermal events were obtained from the analysis of the DSC curves during heating and cooling runs. Thermo-gravimetric analysis (TGA) was done to observe any mass loss or gain due to decomposition or oxidation. This did not occur because none of the measurements showed fluctuation in the TGA curve. The microstructural study of the alloys was done by light optical microscopy, scanning electron microscopy (SEM) and wave dispersive X-ray spectrometer (WDS). The XRD patterns were acquired using PAN-analytical Xpert Pro powder X-ray diffractometer with a CuKα radiation. The XRD spectrum is acquired from 20 to 120° 2θ with a

Table 4
Ternary invariant points of the Cu–Ni–Y system.

Reaction	Type	Temp. (K)	Cu (at.%)	Ni (at.%)	Y (at.%)
Liquid ⇆ hcp-Y + NiY_3 + NiY	E_1	1024	24.12	7.92	67.96
Liquid ⇆ NiY + Ni_2Y + Cu_2Y (r)	E_2	1077	24.93	36.27	38.80
Liquid ⇆ Cu_2Y (r) + Ni_3Y + (Cu,Ni)Y	E_3	1111	39.48	29.26	31.26
Liquid + Ni_2Y_3 ⇆ NiY_3 + NiY	U_1	1090	0.49	34.10	65.41
Liquid + Cu_2Y (h) ⇆ Cu_2Y (r) + Cu_7Y_2	U_2	1124	70.53	0.21	29.26
Liquid + Cu_7Y_2 ⇆ Cu_2Y (r) + $(Cu,Ni)_4Y$	U_3	1122	61.57	10.07	28.36
Liquid + Ni_7Y_2 ⇆ Ni_3Y + $(Cu,Ni)_4Y$	U_4	1401	28.98	46.02	25.00
Liquid + $Cu_xNi_{4-x}Y$ ⇆ Cu_6Y + Ni_5Y	U_5	1171	82.56	4.21	13.23
Liquid + Ni_5Y ⇆ Cu_6Y + fcc(Cu,Ni)	U_6	1167	83.90	4.96	11.14
Liquid + $Ni_{17}Y_2$ ⇆ Ni_5Y + fcc(Cu,Ni)	U_7	1374	72.73	20.70	6.57
Liquid + Ni_2Y + Ni_3Y ⇆ Cu_2Y (r)	P_1	1112	36.70	31.13	32.17

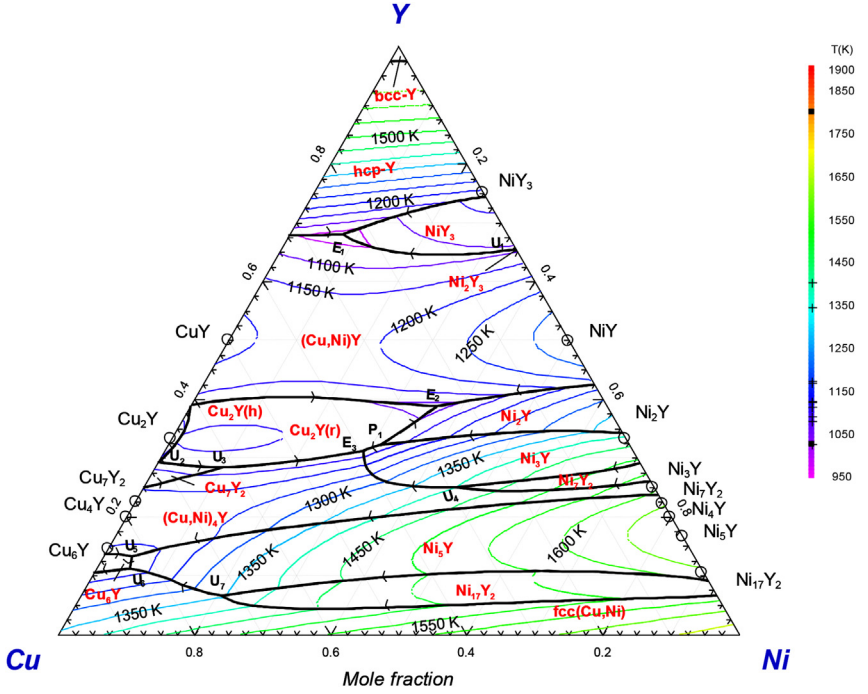

Fig. 3. Calculated liquidus projection of the Cu–Ni–Y system.

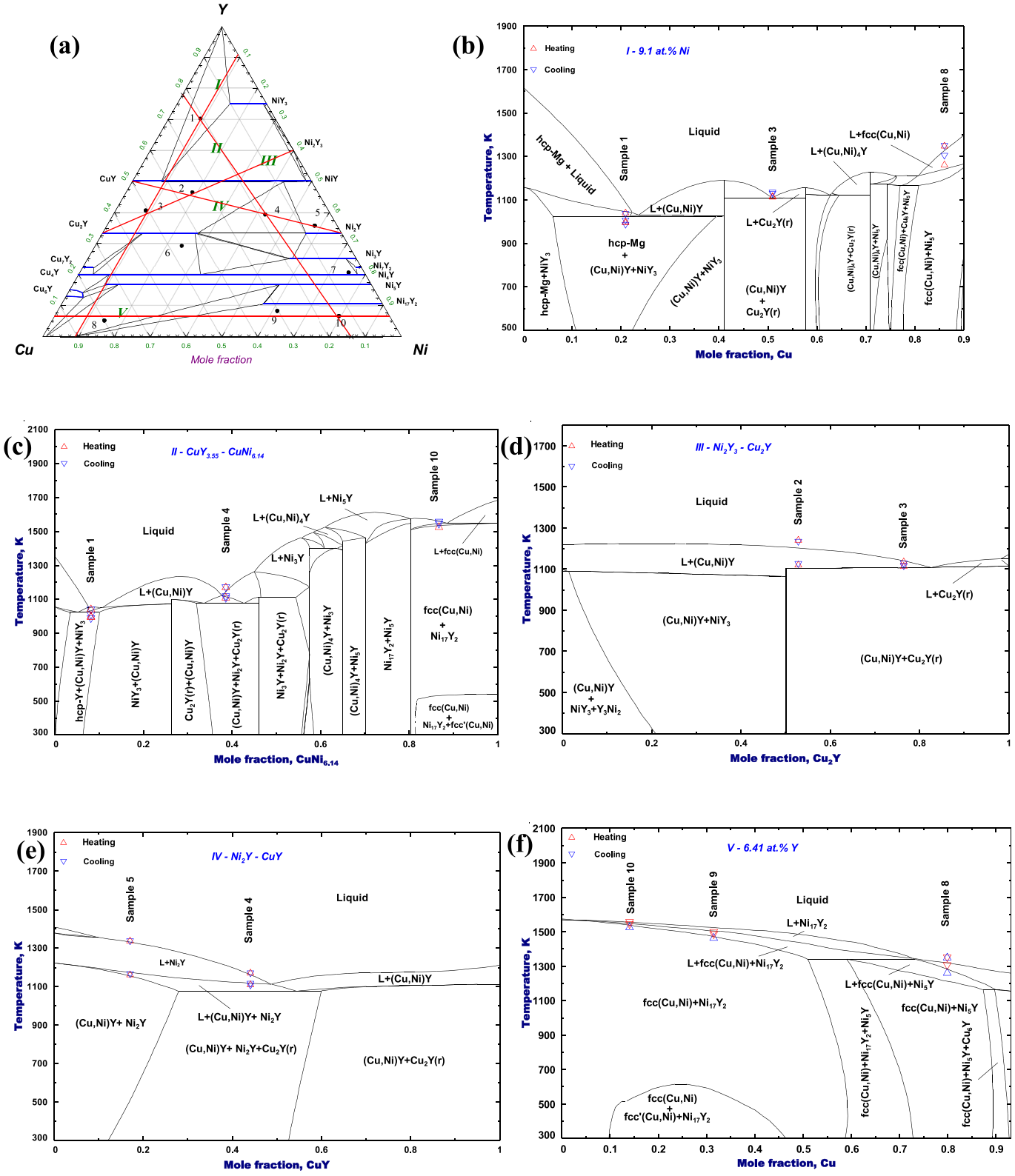

Fig. 4. (a) Isothermal section of the Cu–Ni–Y system showing the lines of the vertical sections; vertical section along (b) constant 9.1 at% Ni; (c) $CuY_{3.55}$-$CuNi_{6.14}$; (d) Ni_2Y_3– Cu_2Y; (e) Ni_2Y– CuY; (f) constant 6.41 at% Y.

Table 5
DSC measurements and calculated transformation temperature of the investigated samples (h & c denotes heating & cooling).

Sample No/ Composition	Equilibrium phases using XRD and WDS	Transformation temperature (K)		Reaction or phase boundary
		Exp.	Cal.	
1. $Cu_{20.8}Ni_{9.1}Y_{70.1}$	hcp-Y	1038(c)/1042(h)	1087	L/L + hcp-Mg
	NiY_3	1008(c)/999(h)	1045	L + hcp-Mg/L + hcp-Mg + NiY_3
	(Cu,Ni)Y	987(c)/995(h)	1024	L + hcp-Mg + NiY_3/hcp-Mg + NiY_3 + (Cu,Ni)Y
2. $Cu_{34.9}Ni_{18.7}Y_{46.4}$	(Cu,Ni)Y	1236(c)/1242(h)	1181	L/L + (Cu,Ni)Y
	Cu_2Y	1127(c)/1121(h)	1103	L + (Cu,Ni)Y/Cu_2Y <R> + (Cu,Ni)Y
3. $Cu_{50.8}Ni_{8.7}Y_{40.5}$	(Cu,Ni)Y	1130(c)/1117(h)	1114	L/L + (Cu,Ni)Y
	Cu_2Y	1136(c)/1114(h)	1109	L + (Cu,Ni)Y/Cu_2Y <R> + (Cu,Ni)Y
4. $Cu_{18.2}Ni_{42.7}Y_{39.1}$	Cu_2Y	1170(c)/1172(h)	1149	L/L + Ni_2Y
	Ni_2Y	1118(c)	1112	L + Ni_2Y/L + (Cu,Ni)Y + Ni_2Y
	(Cu,Ni)Y	1108(c)/1110(h)	1077	L + (Cu,Ni)Y + Ni_2Y/L+(Cu,Ni)Y + Ni_2Y + Cu_2Y<R>
5. $Cu_{6.2}Ni_{58.2}Y_{35.6}$	(Cu,Ni)Y	1338(c)/1337(h)	1329	L/L + Ni_2Y
	Ni_2Y	–	1174	L + Ni_2Y/L + (Cu,Ni)Y + Ni_2Y
		1166(c)/1161(h)	1154	L + Ni_2Y/(Cu,Ni)Y + Ni_2Y
6. $Cu_{46.5}Ni_{24.4}Y_{29.1}$	Cu_2Y	1200(c)/1202(h)	1150	L/L + $(Cu,Ni)_4Y$
	$(Cu,Ni)_4Y$	1167(c)/1169(h)	1115	L + $(Cu,Ni)_4Y$/$(Cu,Ni)_4Y$ + Cu_2Y<R>
7. $Cu_{5.0}Ni_{74.9}Y_{20.1}$	Ni_3Y	1631(h)	1641	L/L + Ni_5Y
	$(Cu,Ni)_4Y$	1586(h)	1573	L + Ni_5Y/L + Ni_5Y +$(Cu,Ni)_4Y$
		1581(h)	1550	L + Ni_5Y + $(Cu,Ni)_4Y$/L + $(Cu,Ni)_4Y$
		1535(h)	1526	L + $(Cu,Ni)_4Y$/Ni_7Y_2 + $(Cu,Ni)_4Y$
8. $Cu_{80.9}Ni_{14.1}Y_{5.0}$	Ni_5Y	1352(c)/1350(h)	1347	L/L + fcc(Cu,Ni)
	fcc(Cu,Ni)	–	1292	L + fcc(Cu,Ni)/L + fcc(Cu,Ni) + Ni_5Y
		1306(c)/1262(h)	1228	L + fcc(Cu,Ni) + Ni_5Y/fcc(Cu,Ni) + Ni_5Y
9. $Cu_{30.3}Ni_{61.6}Y_{8.1}$	fcc(Cu,Ni)	1499(c)	1535	L/L + $Ni_{17}Y_2$
	$Ni_{17}Y_2$	–	1481	L + $Ni_{17}Y_2$/L + $Ni_{17}Y_2$ + fcc(Cu,Ni)
		1485(c)/1466(h)	1447	L + $Ni_{17}Y_2$ + fcc(Cu,Ni)/fcc(Cu,Ni) + $Ni_{17}Y_2$
10. $Cu_{14.0}Ni_{79.6}Y_{6.4}$	fcc(Cu,Ni)	1557(c)	1553	L/L + $Ni_{17}Y_2$
	$Ni_{17}Y_2$	–	1545	L + $Ni_{17}Y_2$/L + $Ni_{17}Y_2$ + fcc(Cu,Ni)
		1544(c)/1526(h)	1536	L + $Ni_{17}Y_2$ + fcc(Cu,Ni)/fcc(Cu,Ni) + $Ni_{17}Y_2$

0.02° step size. XRD analysis of the samples is carried out using X'Pert HighScore Plus Rietveld analysis software.

5. Results and discussion

5.1. Thermodynamic optimization results and discussion

All the thermodynamic calculations in this work have been carried out using FactSage thermodynamic software [82]. The optimized parameters for the constituent binary systems have been taken from the authors previous thermodynamic assessments on the Mg–Ni–Y [11], Mg–Cu–Y [12] and Mg–Cu–Ni [13] systems. However, in a recent publication by Mezbahul-Islam and Medraj [10] many of the binary compounds in the Ni–Y and Cu–Y binaries were reported to have ternary solubility in the Cu–Ni–Y system. In order to reproduce the experimental ternary solubility, the binary intermetallic compounds have been remodeled using the sublattice model instead of the stoichiometric model that was used earlier. Therefore, small adjustment of the model parameters of the intermetallic compounds from the earlier assessments [11–13] was necessary. A self-consistent set of parameters for all the phases in the Cu–Ni–Y system is listed in Tables 1 and 2.

As mentioned earlier, several binary compounds in the Cu–Y and Ni–Y systems have been found to have significant ternary solubility in the Cu–Ni–Y system. The solubility of Cu and Ni in the Ni–Y and Cu–Y binary compounds have been modeled using two sublattices with Y occupying the first lattice. The atomic size of Cu and Ni are very similar. These two elements replace each other and their mixing is allowed on the second sublattice, such as: $(Y\%)_x(Ni\%,Cu\%)_y$ where x and y are the site fractions. Using this model, five compounds: (Y%) (Ni%,Cu)$_5$, (Y%)$_2$(Ni%,Cu)$_7$, (Y%) (Ni%,Cu)$_3$, (Y%) (Ni%,Cu)$_2$ and (Y%)$_3$(Ni%,Cu) in the Ni–Y system and two compounds: (Y%) (Cu%,Ni)$_2$ and (Y%)$_2$(Cu%,Ni)$_7$ in the Cu–Y system have been described. Each of these models has two end members: ${}^oG^{\varphi}_{Y:Ni}$ and ${}^oG^{\varphi}_{Y:Cu}$ where φ is the phase of interest. One of them represents the actual stoichiometry of the compound and the other is a hypothetical end member. The enthalpy and entropy of formation of the actual compound have been taken from the literature whereas for the hypothetical end member they are determined in this work. For example, Ni_7Y_2 has two end members: $G^{Ni_7Y_2}_{Y:Ni}$ and $G^{Ni_7Y_2}_{Y:Cu}$ where the first 'G' represents the actual compound, Ni_7Y_2 in the Ni–Y binary and the second 'G' is the hypothetical end member, Cu_7Y_2. It may be noted that Cu_7Y_2 is also a stable compound in the Cu–Y binary system as can be seen in Fig. 1(b). Therefore, while optimizing Ni_7Y_2 the enthalpy of formation of the hypothetical end member, Cu_7Y_2 has been kept larger than that of the same compound in the Cu–Y system to avoid unwanted formation. However, the entropy of formation was kept the same in both models. Hence, the Cu solubility in Ni_7Y_2 has been obtained mainly using the interaction parameter, ${}^oL^{Ni_7Y_2}_{Y:Ni,Cu}$. The optimized parameters are listed in Table 2. A reverse technique has been used to obtain the Ni solubility in Cu_7Y_2 where Ni_7Y_2 is the hypothetical end member. The same approach has been applied to similar elemental ratio compounds; Cu_2Y and Ni_2Y.

The complete mutual solubility of (Cu,Ni)Y and $(Cu,Ni)_4Y$ have been described using (Y%) (Cu, Ni) and (Y%) (Cu, Ni)$_4$ sublattices. The end members of these two models are: ${}^oG^{(Cu,Ni)Y}_{Y:Cu}$, ${}^oG^{(Cu,Ni)Y}_{Y:Ni}$, ${}^oG^{(Cu,Ni)_4Y}_{Y:Cu}$ and ${}^oG^{(Cu,Ni)_4Y}_{Y:Ni}$ and they represent the actual compounds: CuY, NiY, Cu_4Y and Ni_4Y in their respective binary systems. Since all the compounds are stable in the Cu–Y and Ni–Y phase diagrams as can be seen in Fig. 1(a and b), their enthalpy and entropy of formation was kept the same as the binary systems. Therefore, the complete mutual solubility, (Cu,Ni)Y and $(Cu,Ni)_4Y$ have been described mainly using the interaction parameters, ${}^oL^{(Cu,Ni)Y}_{Y:Cu,Ni}$ and ${}^oL^{(Cu,Ni)_4Y}_{Y:Cu,Ni}$.

$Ni_{17}Y_2$ has been modeled using a four sublattice model as: (Y%)$_2$(Ni%,Cu)$_{12}$(Ni%,Cu)$_3$(Ni%,Cu)$_2$. It was not possible to reduce the number of sublattices using the crystallographic information such as coordination number, Wyckoff positions and symmetry as suggested by Kumar et al. [83]. This model has eight end members as

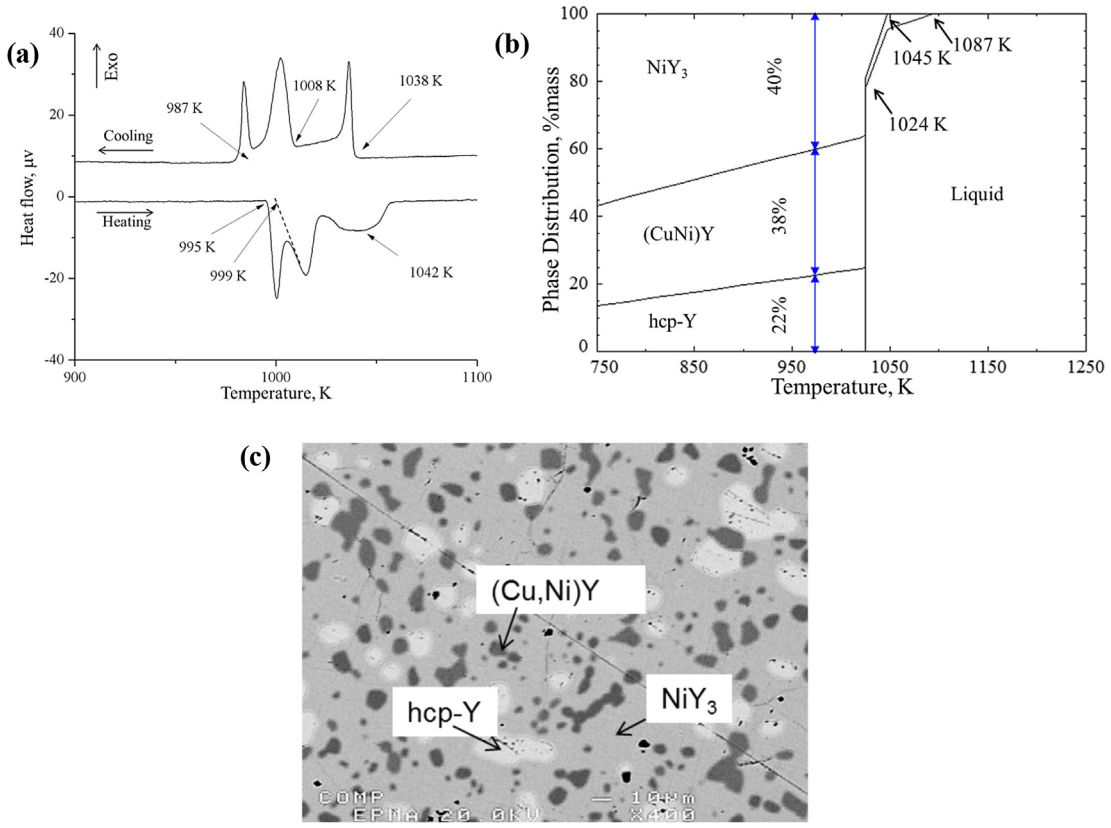

Fig. 5. (a) DSC spectra during heating and cooling; (b) phase assemblage diagram; (c) BSE image [6] of sample 1 (20.8/9.1/70.1 Cu/Ni/Y at.%).

listed in Table 2, where ${}^{o}G^{Ni_{17}Y_2}_{Ni:Ni:Ni:Y}$, represents the actual binary compound $Ni_{17}Y_2$ in the Ni–Y system. All other end members are hypothetical and their Gibbs energy values are determined in this work. However, three of the end members: ${}^{o}G^{Ni_{17}Y_2}_{Ni:Cu:Cu:Y}$, ${}^{o}G^{Ni_{17}Y_2}_{Cu:Ni:Ni:Y}$ and ${}^{o}G^{Ni_{17}Y_2}_{Cu:Ni:Cu:Y}$ have less influence on determining the solubility. Hence, they have been assigned a large positive value of 5000 J/mole. Three ternary interaction parameters have been used to reproduce the ternary solubility closely.

Cu_6Y has ~2 at% solid solubility in the Cu–Y binary system as can be seen in Fig. 1(b). This has been thermodynamically described using a two sublattice model $(Cu\%)_5(Y\%, Cu_2,)$ by Mezbahul-Islam et al. [12] for the binary system. However, Cu_6Y has also been found to have ternary solubility [9,10]. Therefore, to obtain the solubility, Ni is allowed to mix in the second sublattice as: $(Cu\%)_5(Y\%, Cu_2, Ni)$. The model has six end members as listed in Table 2. The enthalpy of four of them, ${}^{o}G^{Cu_6Y}_{Cu:Ni}$, ${}^{o}G^{Cu_6Y}_{Ni:Cu_2}$, ${}^{o}G^{Cu_6Y}_{Ni:Y}$ and ${}^{o}G^{Cu_6Y}_{Ni:Ni}$ have been determined in this work in order to be consistent with the experimental solubility limit. Also, two ternary interaction parameters have been used.

Ni_2Y_3 and $Cu_2Y(h)$ have been described using the stoichiometric model as no ternary solubility has been reported in the literature or could be observed in the current work. $Cu_2Y(h)$ is a metastable compound which stabilizes above 1116 K as can be seen in Fig. 1(b). The enthalpy and entropy of formation of these two compounds have been taken from previous assessments [11,12].

In order to be consistent with the DSC experimental data, two excess ternary Gibbs energy terms, $g^{ijk}_{CuY(Ni)}$ and $g^{ijk}_{NiY(Cu)}$ have been used for the liquid phase. The $g^{ijk}_{CuY(Ni)}$ parameter is related to the influence of Ni on the Cu–Y bonding energy whereas $g^{ijk}_{NiY(Cu)}$ is the influence of Cu on the Ni–Y bonding energy in the ternary liquid. The binary and ternary liquid parameters are listed in Table 1.

The calculated isothermal section of the Cu–Ni–Y system at 973 K is shown in Fig. 2 in relation to the available experimental data from [9,10]. The arrow heads point to the phases that are present in the alloy. It can be seen that the present calculation can reproduce the phase equilibrium with great accuracy. A comparison between the experimental and thermodynamic calculation of the ternary solubility of the binary compounds is given in Table 3. It showed acceptable agreement except for Ni_7Y_2. The solubility limit of this compound has been obtained through five spot WDS measurements of one sample by Mezbahul-Islam and Medraj [10] which showed scattered data with standard deviation of 0.99 at%. Hence, lower weight has been given to the maximum solubility limit of Ni_7Y_2 during optimization.

The calculated liquidus projection of the Cu–Ni–Y system is shown in Fig. 3. The thicker solid lines represent the liquid compositions involved in the univariant three-phase equilibria. The areas enclosed by the univariant lines and the sides of Gibbs triangle represent the primary crystallization fields of different phases. Three consecutive univariant lines intersect at a four-phase invariant point (i.e. ternary eutectic, peritectic or quasi-peritectic point). According to the present calculation Cu–Ni–Y system has seven quasi-peritectic, one peritectic and three ternary eutectics. The respective reactions of these points are listed in Table 4. The liquidus projection in Fig. 3 is divided into sixteen primary crystallization fields: hcp-Y, bcc-Y, NiY_3, Ni_2Y_3, (CuNi)Y, $Cu_2Y(r)$, $Cu_2Y(h)$, Ni_2Y, Cu_7Y_2, Ni_3Y, Ni_7Y_2, $(CuNi)_4Y$, Cu_6Y, Ni_5Y, $Ni_{17}Y_2$ and fcc(Cu, Ni). Relatively flat liquidus can be seen near CuY–NiY section of the projection in Fig. 3. This can be attributed to the close melting temperature of CuY (1209 K) and NiY (1329 K) and to their mutual solubility.

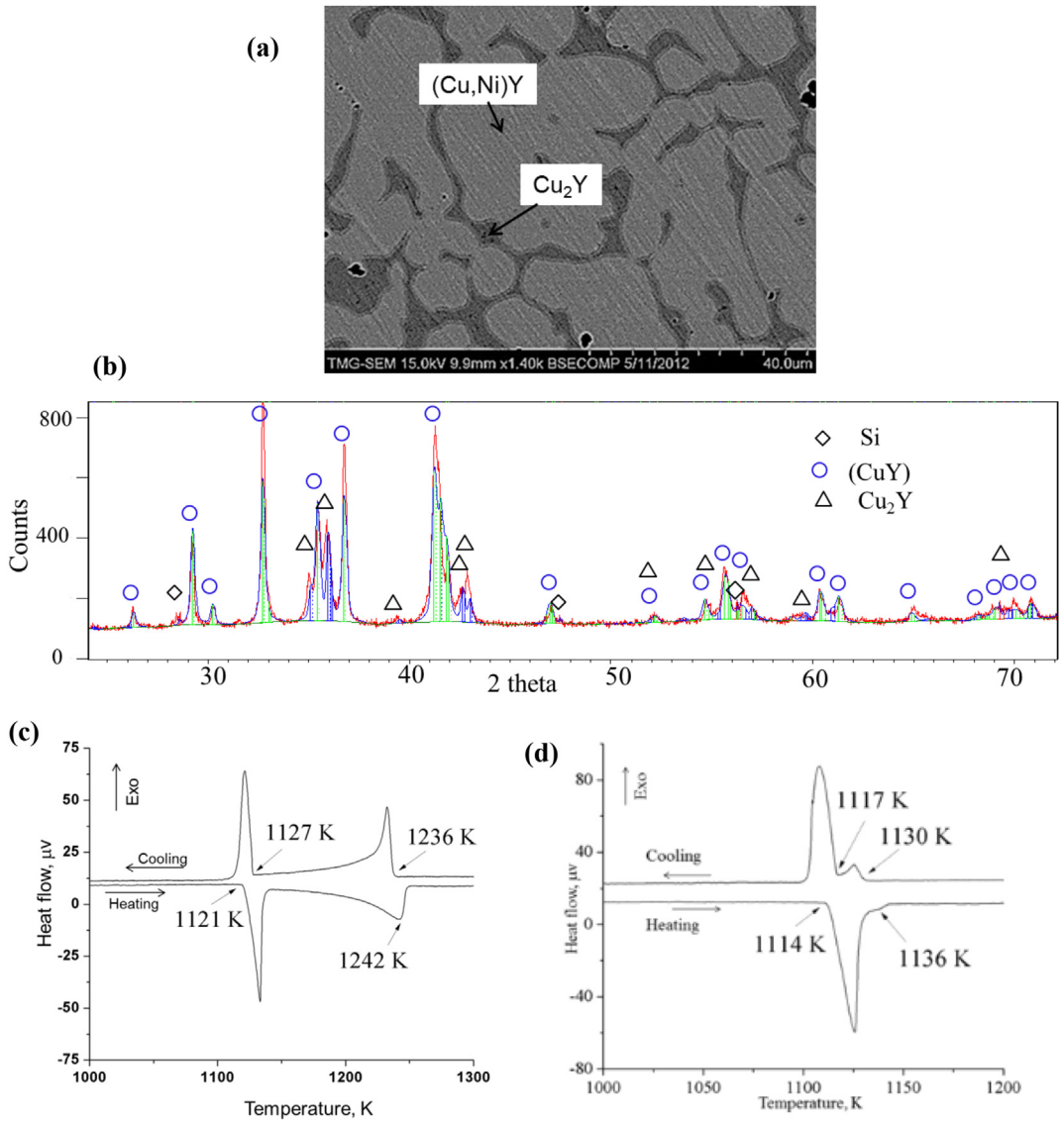

Fig. 6. (a) BSE image; (b) XRD pattern of sample 2; DSC spectra of (c) sample 2 (34.9/18.7/46.4 Cu/Ni/Y at.%) and) sample 3 (50.8/8.7/40.5 Cu/Ni/Y at.%).

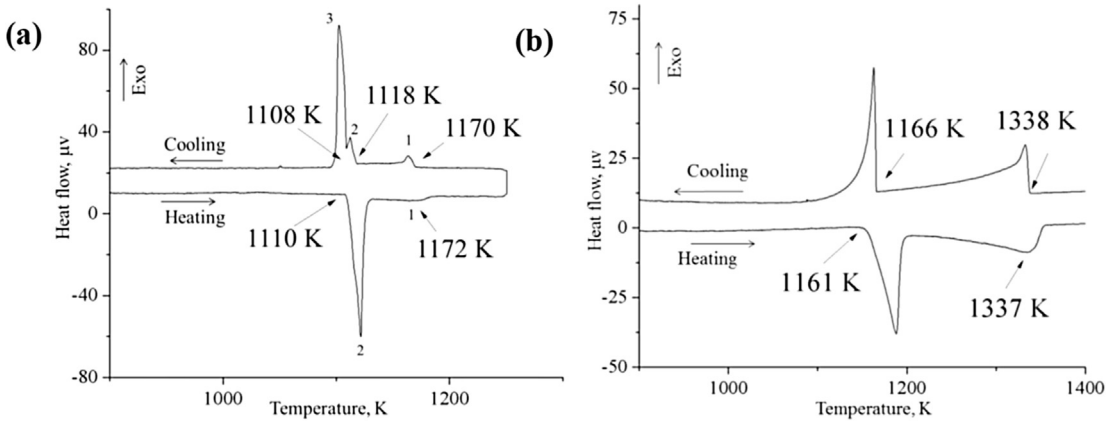

Fig. 7. DSC spectra of (a) sample 4 (18.2/42.7/39.1 Cu/Ni/Y at.%); (b) sample 5 (6.2/58.2/35.6 Cu/Ni/Y at.%) during heating and cooling.

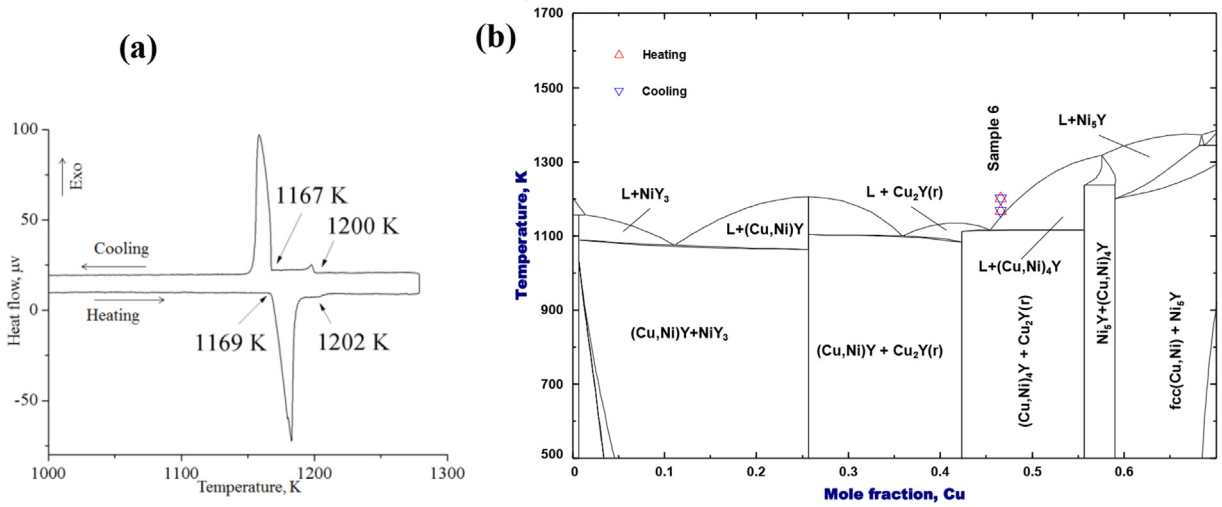

Fig. 8. (a) DSC spectra during heating and cooling; (b) Calculated vertical section at 24.4 at% Ni with DSC signals of sample 6 (46.5/24.4/29.1 Cu/Ni/Y at.%).

5.2. Comparison between experimental results and thermodynamic modeling

Five vertical sections are presented in Fig. 4. The compositions of these sections are shown in Fig. 4(a). They are selected to give a detailed understanding of the phase equilibria in the Cu–Ni–Y system from room temperature to the liquidus. Also, these vertical sections consist of at least two key samples of which DSC measurements have been performed in this work. This will provide a better understanding of the liquidus. All the vertical sections show good agreement with the DSC thermal arrests. The ternary solubility of the binary compounds is temperature dependent. For this reason, some of the phase boundaries are found to be skewed at higher temperatures. Flat liquidus surfaces can be seen in the vertical sections *I* and *III*, in Fig. 4(d) and (e). This is due to the close melting temperature of the binary compounds: Ni_2Y, Cu_2Y CuY and NiY. The composition of the key samples, the detected thermal arrests and relevant phase transformation reactions are listed in Table 5. Detailed analysis of the DSC spectra is given in section 5.3.

5.3. Analysis of the DSC spectra

Sample 1 (20.8/9.1/70.1 Cu/Ni/Y at.%) is located in the three-phase region: hcp-Y + NiY_3 + (Cu,Ni)Y. The DSC spectra of this alloy are shown in Fig. 5(a). The heating profile shows three thermal events at 1042, 999 and 995 K that reoccurred in the cooling at 1038, 1008 and 987 K. These measured temperatures can be correlated to the calculated vertical sections in Fig. 4(b) and (c) which show good agreement. The DSC results of the same alloy have been used in two vertical sections that represent two different sides of the phase diagram. This approach gives a clear viewing of the melting behavior of the alloy. Fig. 5(b) shows the phase assemblage diagram of sample 1, where the relative mass versus temperature is calculated. The proportion of each phase at any temperature of interest can easily be interpreted from this diagram. For instance, at 973 K which is the annealing temperature, 100 g of the overall material consists of 22 g of hcp-Y, 38 g of (CuY) and 40 g of NiY_3. Fig. 5(b) also shows that the first solid starts to precipitate at 1087 K in the form of hcp-Y and continues till the end of the solidification at 1024 K. This phase (hcp-Y) can be seen as the white precipitates in the microstructure in Fig. 5(c). The visual inspection of the phases in the microstructure shows that approximately one fifth of the total phase amount in the microstructure is hcp-Y which is in accord with the thermodynamic calculation. The grey matrix and the dark islands in the microstructure in Fig. 5(c) is NiY_3 and (Cu,Ni)Y, respectively. According to the present calculation, the solidification of these two phases occur at 1045 K for NiY_3 and 1024 K for (Cu,Ni)Y.

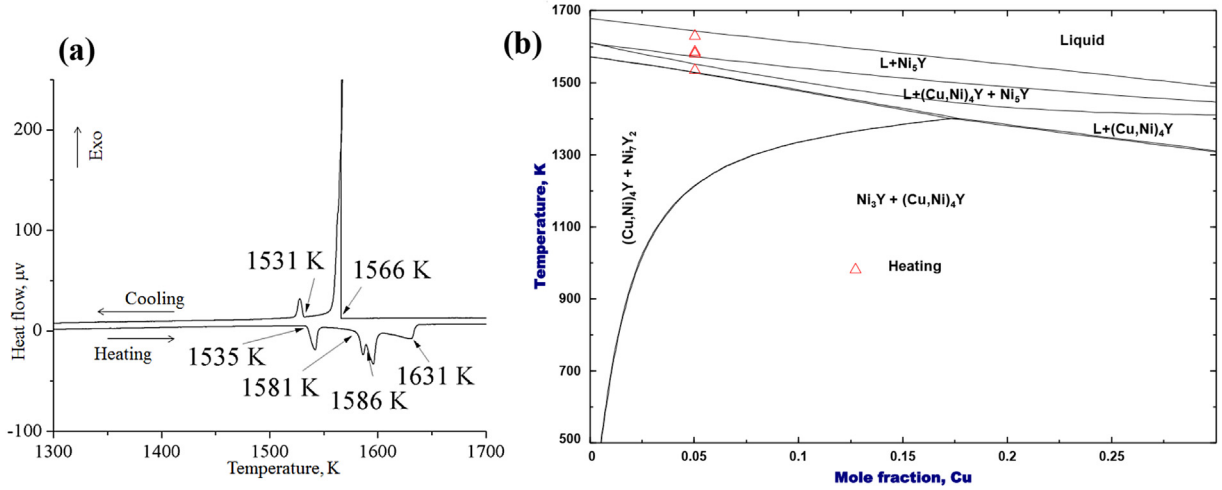

Fig. 9. (a) DSC spectra; (b) Calculated vertical section at 20.1 at% Y with DSC signals of sample 7 (5.0/74.9/20.1 Cu/Ni/Y at.%).

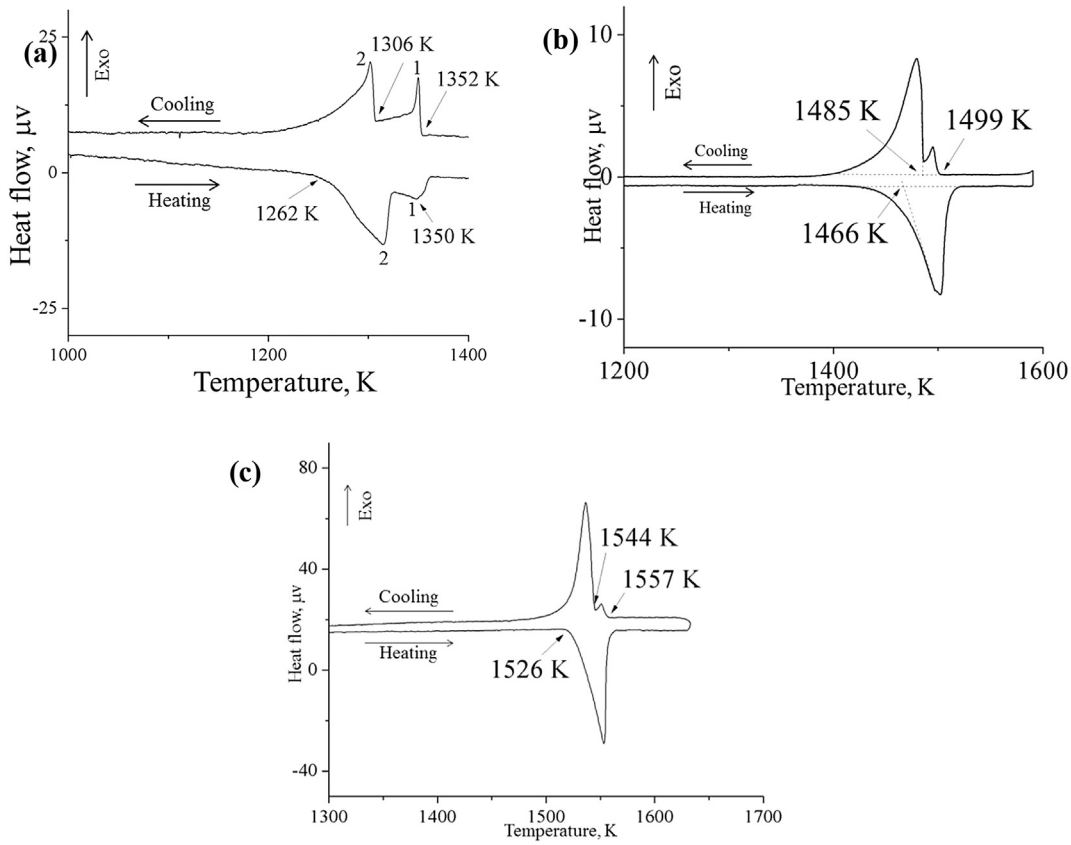

Fig. 10. DSC spectra of (a) sample 8 (80.9/14.1/5.0 Cu/Ni/Y at.%); (b) sample 9 (30.3/61.6/8.1 Cu/Ni/Y at.%); (c) sample 10 (14.0/79.6/6.4 Cu/Ni/Y at.%) during heating and cooling.

Both samples 2 (34.9/18.7/46.4 Cu/Ni/Y at.%) and 3 (50.8/8.7/40.5 Cu/Ni/Y at.%) are located in the two-phase region: (Cu,Ni)Y + Cu_2Y. The BSE image of sample 2 in Fig. 6(a) shows these two phases. The grey matrix in the microstructure is (Cu,Ni)Y and the dark network is Cu_2Y. The XRD pattern in Fig. 6(b) positively identifies these compounds. The DSC spectra of these alloys are shown in Fig. 6(c) and (d). Both of them show two thermal events during heating which reoccurred during cooling. The thermal arrests are projected on the vertical section along Cu_2Y–Ni_2Y_3 in Fig. 4(d) which shows reasonable agreement. According to the present calculation the liquid in this part of the alloy system is quite flat. In order to verify the slope of the liquidus, these two alloys have been chosen for the DSC experiment. The slope of the liquidus during optimization has been calibrated based on these measurements.

The DSC spectra of sample 4 (17.4/43.5/39.1 Cu/Ni/Y at.%) with the heating and cooling runs are shown in Fig. 7(a). Two peaks during heating and three peaks during cooling are observed. It can be seen that the 2nd peak during heating overlapped with the 3rd peak. Areas under the curve between the last two cooling peaks (−125 J/g) and the 2nd heating peak (123 J/g) are similar which confirms that the heating peak is in fact two overlapping peaks. Similar results were observed in all the three heating and cooling cycles. The thermal arrests observed during cooling are at temperatures of 1170, 1118 and 1108 K. While during heating, the peaks' temperatures are 1172 and 1110 K. The DSC thermal arrests are projected on the calculated vertical section Ni_2Y–CuY as can be seen in Fig. 4(e). The liquidus temperature is found at 1149 K while the experimental value is 1170 K. The other two thermal events in

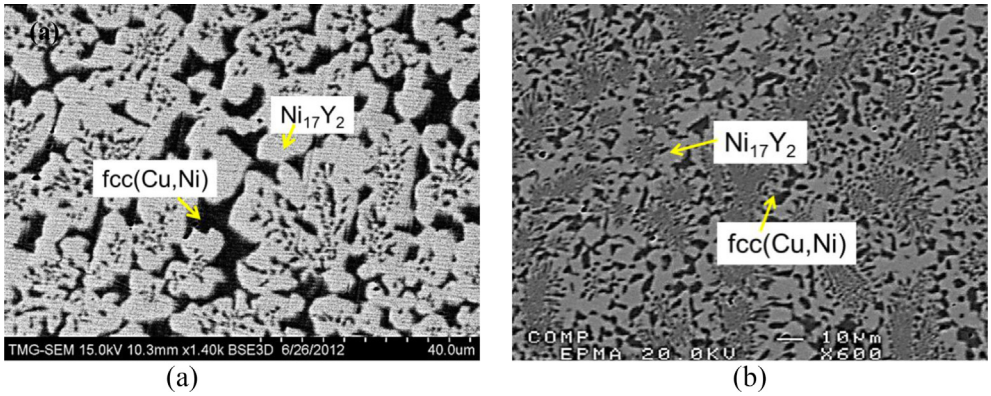

Fig. 11. BSE image of (a) sample 9 (30.3/61.6/8.1 Cu/Ni/Y at.%); (b) sample 10 (14.0/79.6/6.4 Cu/Ni/Y at.%).

the DSC spectra are due to the phase transformations; L + Ni_2Y/L + Ni_2Y + (Cu,Ni)Y and L + Ni_2Y + (Cu,Ni)Y/Cu_2Y + Ni_2Y + (Cu,Ni)Y. According to the calculation these transformations occur at 1112 and 1077 K. Similar DSC result has been observed for sample 5 (6.2/58.2/35.6 Cu/Ni/Y at.%) with two thermal events as can be seen in Fig. 7(b). The vertical section along Ni_2Y–CuY in Fig. 4(e) shows that the slope of the liquid is little bit steeper in the Ni–Y side than in the Cu–Y side. Therefore, the liquidus projection in Fig. 3 showed closely associated liquidus lines near the Ni–Y side of the Cu–Ni–Y system.

Sample 6 (46.5/24.4/29.1 Cu/Ni/Y at.%) is prepared in the two phase region of $(Cu,Ni)_4Y$ + Cu_2Y as can be seen in Fig. 4(a). The DSC spectra in Fig. 8(a) show two thermal events at 1202 and 1169 K in the heating cycle which reoccurred at 1200 and 1167 K during cooling cycle. The DSC signals have been projected on the calculated vertical section at constant 24.4 at% Ni as can be seen in Fig. 8(b). The difference between the calculation and experimental measurement is about 50 K. It was not possible to improve the consistency with this particular alloy without worsening the consistency in other parts of the phase diagram. Hence, it is decided to accept this amount of error.

DSC results of sample 7 (5.0/74.9/20.1 Cu/Ni/Y at.%) in Fig. 9(a) show four thermal events in the heating spectrum. However, only two peaks appear in the cooling cycle. This is probably due to the supercooling effect which shifts the cooling peaks. Several phase transformations occur in a relatively narrow and sufficiently high temperature range which forces the first three peaks during cooling to overlap and appear as one large peak. Similar spectrum has been observed in all three DSC runs of the sample. Therefore, only the heating signals will be considered for this alloy. Fig. 9(b) shows the calculated vertical section at 20.1 at% Y with the DSC signals of this sample. The measured transformation temperatures correspond well with the phase boundaries in the vertical section: L/L + Ni_5Y/L + Ni_5Y + $(Cu,Ni)_4Y$/L + $(Cu,Ni)_4Y$/Ni_3Y + $(Cu,Ni)_4Y$ occurring at 1641, 1573, 1550 and 1526 K predicted from thermodynamic calculation, respectively.

The DSC spectra of samples 8 (80.9/14.1/5.0 Cu/Ni/Y at.%), 9 (30.3/61.6/8.1 Cu/Ni/Y at.%) and 10 (14.0/79.6/6.4 Cu/Ni/Y at.%) are shown in Fig. 10(a–c). All of them show similar feature of two peaks in a small temperature range. However, it can be noticed that the liquidus temperature increases with increasing Ni concentration in samples 8 to 10. The calculated vertical section along constant 6.4 at % Y in Fig. 4(f) shows good agreement with the experimental measurements. Both samples 9 and 10 are located in the fcc(Cu,Ni) + $Ni_{17}Y_2$ phase field as shown in Fig. 4(a). The BSE images of these alloys in Fig. 11(a) and (b) clearly show the two-phase equilibrium. The dark and white morphologies in the microstructures are fcc(Cu,Ni) and $Ni_{17}Y_2$, respectively. However, the dark grey region in the microstructure of sample 10 is not a separate phase but an alternating layered structure of fcc(Cu,Ni) and $Ni_{17}Y_2$. Sample 9 also shows this type of morphology. But the layers in sample 9 are thicker than in sample 10. According to the liquidus projection, shown in Fig. 3, these alloys are located near a univariant valley causing this eutectic structure to occur.

A detailed analysis of the DSC spectra of the 10 key samples has been provided in this section. The discussion is associated with the thermodynamic calculations (vertical sections, phase assemblage diagram) to give better understanding of the phase relationships at different compositions with temperature. The thermodynamic calculations show consistency with most of the DSC measurements. However, two samples (1 and 6) show significant difference in the liquidus temperature (up to ~50 K) from the thermodynamic calculations. Unfortunately, this inconsistency could not be reduced without affecting other parts of the phase diagram.

6. Summary

Thermodynamic modeling of the Cu–Ni–Y ternary system has been carried out for the first time in this work. A self-consistent set of parameters is provided which enables the reproduction of the experimentally verified phase relationships in this system. Ternary solubility of all the binary compounds has been described using sublattice model within the compound energy formalism (CEF) to reproduce the recently reported experimental data. The modified quasi-chemical model (*MQM*) is used to describe the liquid phase to account for the presence of short range ordering. The isothermal section of the Cu–Ni–Y system at 973 K has been calculated which showed very good agreement with the available experimental data. DSC experiments have been carried out on 10 selected key samples to acquire information regarding the melting/freezing and phase transformation temperatures. Detailed discussions of the DSC spectra have been performed to provide better understanding of the melting behavior of the alloys. The results of the DSC have been used during optimization to calibrate the liquidus surface which showed seven quasi-peritectic (U), one peritectic (P) and three ternary eutectic (E) points. The invariant reactions along with the composition and temperature have been provided. Sixteen primary crystallization fields: hcp-Y, bcc-Y, NiY_3, Ni_2Y_3, (CuNi)Y, Cu_2Y(r), Cu_2Y(h), Ni_2Y, Cu_7Y_2, Ni_3Y, Ni_7Y_2, $(CuNi)_4Y$, Cu_6Y, Ni_5Y, $Ni_{17}Y_2$ and fcc(Cu, Ni) have been identified in the liquidus projection.

Appendix A. Supplementary data

Supplementary data related to this article can be found at http://dx.doi.org/10.1016/j.matchemphys.2014.12.032.

References

[1] H. Ma, L.-L. Shi, J. Xu, E. Ma, Chill-cast in situ composites in the pseudo-ternary Mg-(Cu,Ni)-Y glass-forming system: microstructure and compressive properties, J. Mater. Res. 22 (2007) 314–325.
[2] Q.F. Li, K.Q. Qiu, X. Yang, Y.L. Ren, X.G. Yuan, T. Zhang, Glass forming ability and reliability in fracture stress for Mg–Cu–Ni–Nd–Y bulk metallic glasses, Mat. Sci. Eng. A 491 (2008) 420–424.
[3] H. Ma, L.-L. Shi, J. Xu, Y. Li, E. Ma, Improving glass-forming ability of Mg-Cu-Y via substitutional alloying: effects of Ag versus Ni, J. Mater. Res. 21 (2006) 2204–2214.
[4] E.S. Park, D.H. Kim, Formation of Mg-Cu-Ni-Ag-Zn-Y-Gd bulk glassy alloy by casting into cone-shaped copper mold in air atmosphere, J. Mater. Res. 20 (2005) 1465–1469.
[5] C. Shaw, H. Jones, The contributions of different alloying additions to hardening in rapidly solidified magnesium alloys, Mater. Sci. Eng. A, A 226–228 (1997) 856–860.
[6] M. Mezbahul-Islam, M. Medraj, Phase equilibrium in Mg-Cu-y, Sci. Rep. 3 (2013) 3033.
[7] V.V. Burnasheva, B.P. Tarasov, Effect of the partial replacement of nickel or yttrium by other metals on hydrogen absorption by yttrium-nickel (YNi_3) compounds, Zh. Neorg. Khim. 29 (1984) 1136–1141.
[8] P.D. Carfagna, W.E. Wallace, R.S. Craig, Crystallographic, Magnetic, Characteristics of the Y_2 $Ni_{17-x}Cu_x$ System, J. Solid State Chem. 2 (1970) 1–5.
[9] L. Zheng, J. Nong, A part of room temperature section of phase diagram of Y-Cu-Ni (Y ≤ 16.7 at.%) system, Acta Metall. Sin. 21 (1985) B58–B60.
[10] M. Mezbahul-Islam, M. Medraj, Experimental study of the Cu–Ni–Y system at 700°C using diffusion couples and key alloys, J. Alloys Compd. 561 (2013) 161–173.
[11] M. Mezbahul-Islam, M. Medraj, A critical thermodynamic assessment of the Mg-Ni, Ni-Y binary and Mg-Ni-Y ternary systems, Calphad 33 (2009) 478–486.
[12] M. Mezbahul-Islam, D. Kevorkov, M. Medraj, The equilibrium phase diagram of the magnesium–copper–yttrium system, J. Chem. Thermodyn. 40 (2008) 1064–1076.
[13] M. Mezbahul-Islam, M. Medraj, Thermodynamic modeling of the Mg-Cu-Ni ternary system using the modified quasichemical model, in: M. Favard, G. Dufour (Eds.), Conference of Metallurgists (COM), Metsoc, Montreal, 2011, pp. 241–253.
[14] B.J. Beaudry, A.H. Daane, Yttrium-nickel system, Trans. Metall. Soc. AIME 218 (1960) 854–859.
[15] R.F. Domagala, J.J. Rausch, D.W. Levinson, The systems Y-Fe, Y-Ni, and Y-Cu, Trans. Am. Soc. Met. 53 (1961) 137–155.
[16] K.H.J. Buschow, Intermetallic compounds of rare earth and 3d transition

metals, Rep. Prog. Phys. 40 (1977) 1179–1256.
[17] P. Nash, Y. Ni-, Binary Alloy Phase Diagrams, second ed., ASM International, Materials Park, OH, 1991.
[18] P.R. Subramanian, J.F. Smith, Thermodynamics of formation of yttrium-nickel alloys, Metall. Trans. B 16B (1985) 577–584.
[19] Z. Du, W. Zhang, Thermodynamic assessment of the Ni-Y system, J. Alloys Compd. 245 (1996) 164–167.
[20] N. Mattern, M. Zinkevich, W. Loeser, G. Behr, J. Acker, Experimental and thermodynamic assessment of the Nb-Ni-Y system, J. Phase Equilibr. Diffus. 29 (2008) 141–155.
[21] M.H.H. Van, K.H.J. Buschow, A.R. Miedema, Hydrogen absorption of rare-earth (3d) transition intermetallic compounds, J. Less-Common Met. 49 (1976) 473–475.
[22] A.R. Miedema, On the heat of formation of solid alloys. II, J. Less-Common Met. 46 (1976) 67–83.
[23] R.E. Watson, L.H. Bennett, Optimized predictions for heats of formation of transition-metal alloys. II, Calphad 8 (1984) 307–321.
[24] G.I. Batalin, V.A. Stukalo, N.Y. Neshchimenko, V.A. Gladkikh, O.I. Lyuborets, Enthalpy of formation of molten yttrium-nickel alloys, Izv. Akad. Nauk. SSSR, Met. (1977) 44–45.
[25] S.G. Fries, H.L. Lukas, R. Konetzki, R. Schmid-Fetzer, Experimental investigation and thermodynamic optimization of the Y-Cu binary system, J. Phase. Equil. 15 (6) (1994) 606–614.
[26] U. Abend, H.J. Schaller, Constitution and thermodynamics of Cu-Y alloys, Berichte Bunsen-Gesellschaft 101 (1997) 741–748.
[27] T.B. Massalski, J.L. Murray, L.H. Bennett, H. Barker, Binary Alloy Phase Diagrams: Cu-Y, ASM International, Metals park, Ohio, 1986, pp. 977–978.
[28] H. Okamoto, Cu-Y (copper-yttrium), J. Phase Equilib. 19 (1998) 398–399.
[29] D.J. Chakrabarti, D.E. Laughlin, The Cu–Y (Copper-Yttrium) system, Bull. Alloy Phase Diagr. 2 (1981) 315–319.
[30] G. Qi, K. Itagaki, A. Yazawa, High-temperature heat content measurements of copper-RE (RE = yttrium, lanthanum, cerium, praseodymium, neodymium) binary systems, Mater. Trans. JIM 30 (1989) 273–282.
[31] O.Y. Sidorov, M.G. Valishev, Y.O. Esin, P.V. Gel'd, V.M. Zamyatin, A.Y. Dubrovsky, Partial and integral enthalpies of formation of liquid copper-yttrium and copper-zirconium alloys, Izv. Akad. Nauk. SSSR, Met. (1990) 188–190.
[32] V.S. Sudavtsova, G.I. Batalin, A.V. Kalmykov, I.G. Starchevskaya, Thermodynamic properties of liquid binary alloys of copper with scandium, yttrium, and lanthanum, Izv. Vyssh. Uchebn. Zaved. Tsvetn. Metall. (1985) 98–101.
[33] S. Watanabe, O.J. Kleppa, Thermochemistry of alloys of transition metals: Part IV. Alloys of copper with scandium, yttrium, lanthanum, and lutetium, Metall. Trans. B 15B (1984) 357–368.
[34] V.V. Berezutskii, G.M. Lukashenko, Thermodynamic properties of liquid copper-yttrium alloys, Zh. Fiz. Khim. 61 (1987) 1422–1424.
[35] A. Boudene, K. Hack, A. Mohammad, D. Neuschuetz, E. Zimmermann, G. Effenberg, S. Fries, H.L. Lukas, R.A. Konetzki, Thermochemical measurements and assessment of the phase diagrams in the system Y-Ba-Cu-O, High. Temp. Mater. Sci. 35 (1996) 159–179.
[36] K. Itagaki, G. Qi, M.S. An, P.J. Spencer, Phase diagram and thermochemistry of the copper-yttrium system, Calphad 14 (1990) 377–384.
[37] M. Hansen, K.P. Anderko, Constitution of Binary Alloys, Translated from German, McGraw-Hill Book Co, 1957.
[38] D.J. Chakrabarti, D.E. Laughlin, S.W. Chen, Phase Diagrams of Binary Copper Alloys, ASM International, Ohio, OH, 1994, pp. 276–286.
[39] E. Schuermann, E. Schulz, Liquidus and solidus curves of the systems copper-manganese and copper-nickel, Z. Met. 62 (1971) 758–762.
[40] E.A. Feest, R.D. Doherty, Copper-nickel equilibrium phase diagram, J. Inst. Met. 99 (1971) 102–103.
[41] B. Predel, R. Mohs, Thermodynamic study of molten nickel-copper alloys, Arch. Eisenhut 42 (1971) 575–579.
[42] B. Mozer, D.T. Keating, S.C. Moss, Neutron measurement of clustering in the alloy CuNi [copper-nickel], Phys. Rev. 175 (1968) 868–876.
[43] M.F. Ebel, X-ray measurements on spinodal decomposition in copper-nickel alloys, Phys. Status. Solidi. A 5 (1971) 91–94.
[44] J. Vrijen, S. Radelaar, Clustering in copper-nickel alloys: a diffuse neutron-scattering study, Phys. Rev. B 17 (1978) 409–421.
[45] T. Tsakalakos, Spinodal decomposition in copper-nickel alloys by artificial composition modulation technique, Scr. Metall. 15 (1981) 255–258.
[46] R.N. Dokken, J.F. Elliott, Calorimetry at 1100 to 1200°: the copper-nickel, copper-silver, and copper-cobalt systems, Trans. Metal. Soc. AIME 233 (1965) 1351–1358.
[47] Y. Tozaki, Y. Iguchi, S. Banya, T. Fuwa, Heat of mixing of iron alloys, in: Iron Steel Inst, 1973, pp. 130–132.
[48] Y. Iguchi, Y. Tozaki, M. Kakizaki, Calorimetric Examination of mixing heats of nickel and cobalt alloys, J. Iron Steel Inst. Jap. 63 (1977) 953–961.
[49] U.K. Stolz, I. Arpshofen, F. Sommer, B. Predel, Determination of the enthalpy of mixing of liquid alloys using a high-temperature mixing calorimeter, J. Phase. Equil. 14 (1993) 473–478.
[50] M.A. Turchanin, S.V. Porokhnya, L.V. Belevtsov, A.V. Kokhan, Thermodynamic properties of liquid copper-nickel alloys, Rasplavy (1994) 8–12.
[51] C.W. Schultz, G.R. Zellars, S.L. Payne, E.F. Foerster, Activities of copper and nickel in liquid copper-nickel alloys, Bur. Mines Rep. Invest. 6410 (1964) 9.
[52] A.D. Kulkarni, R.E. Johnson, Thermodynamic studies of liquid copper alloys by electromotive force method. II. Copper-nickel-oxygen and copper-nickel systems, Metal. Trans. 4 (1973) 1723–1727.
[53] V.V. Berezutskii, G.M. Lukashenko, Thermodynamic properties of liquid nickel-copper alloys, Ukr. Khim. Zh. Russ. Ed.) 53 (1987) 1029–1032.
[54] J.S.L. Leach, M.B. Bever, Heats of formation of copper-nickel alloys, Trans. Met. Soc. AIME. 215 (1959) 728–729.
[55] R.A. Oriani, W.K. Murphy, Heats of formation of solid nickel-copper and nickel-gold alloys, Acta Mater. 8 (1960) 23–25.
[56] L. Elford, F. Mueller, O. Kubaschewski, Thermodynamic properties of copper-nickel alloys, Ber. Bunsenges. 73 (1969) 601–605.
[57] A.A. Vecher, Y.I. Gerasimov, Investigation of thermodynamic properties of binary metallic systems by the electromotive force method. VII. Cu-Ni solid solutions, Zh. Fiz. Khim. 37 (1963) 490–498.
[58] R.A. Rapp, F. Maak, Thermodynamic properties of solid copper-nickel alloys, Acta Mater. 10 (1962) 63–69.
[59] I. Katayama, H. Shimatani, Z. Kozuka, Thermodynamic study of solid copper-nickel and nickel-molybdenum alloys by emf. measurements using solid electroyte, J. Jap. Inst. Met. 37 (1973) 509–515.
[60] A. Kontopoulos, Thermodynamic activities in copper-nickel-iron solid solutions, Prakt. tes Akad. Athenon 52 (1978) B607–B619.
[61] S. Srikanth, K.T. Jacob, Thermodynamic properties of copper-nickel alloys: measurements and assessment, Mater. Sci. Technol. 5 (1989) 427–434.
[62] A.M. Sabine, Thermodynamic re-evaluation of the copper-nickel system, Calphad 16 (1992) 255–260.
[63] M.A. Turchanin, P.G. Agraval, A.R. Abdulov, Phase equilibria and thermodynamics of binary copper systems with 3d-metals. VI. Copper-nickel system, Powder Metall. Met. Ceram. 46 (2007) 467–477.
[64] H. Kadomatsu, Y. Kawanishi, M. Kurisu, Structural phase transitions in $YCu_{1-x}\mu_x$ (M = Ni, Ag, and Ga), J. Less. Common Met. 141 (1988) 29–36.
[65] V. Paul-Boncour, A. Lindbaum, E. Gratz, E. Leroy, A. Percheron-Guégan, Structural study of the pseudobinary $Y(Ni,Cu)_2$ system, Intermetallics 10 (2002) 1011–1017.
[66] A.E.D. Ohtani, wight, Crystal structure of R.E.-Ni_4Au compounds and unit cell constants in the YCo_5-YNi_5-YCu_5 series, J. Less. Common Met. 43 (1975) 121–128.
[67] K. Gupta, The Cu-Ni-Y (Copper-Nickel-Yttrium) system, J. Phase Equilibr. Diffus. 30 (2009) 651–656.
[68] A.T. Dinsdale, SGTE data for pure elements, Calphad 15 (1991) 317–425.
[69] A.D. Pelton, S.A. Degterov, G. Eriksson, C. Robelin, Y. Dessureault, The modified quasichemical model I - binary solutions, Metall. Mater. Trans. B 31B (2000) 651–659.
[70] A.D. Pelton, P. Chartrand, The modified quasi-chemical model: Part II. Multicomponent solutions, Metall. Mater. Trans. A 32A (2001) 1355–1360.
[71] P. Chartrand, A.D. Pelton, The modified quasi-chemical model: part III. Two sublattices, Metall. Mater. Trans. A 32A (2001) 1397–1407.
[72] A.D. Pelton, P. Chartrand, G. Eriksson, The modified quasi-chemical model: part IV. Two-sublattice quadruplet approximation, Metall. Mater. Trans. A 32 (2001) 1409–1416.
[73] P.J. Spencer, A.D. Pelton, Y.-B. Kang, P. Chartrand, C.D. Fuerst, Thermodynamic assessment of the Ca–Zn, Sr–Zn, Y–Zn and Ce–Zn systems, Calphad 32 (2008) 423–431.
[74] L.-L. Jin, Y.-B. Kang, P. Chartrand, C.D. Fuerst, Thermodynamic evaluation and optimization of Al-La, Al-Ce, Al-Pr, Al-Nd and Al-Sm systems using the modified quasichemical model for liquids, Calphad 35 (2011) 30–41.
[75] Y.-B. Kang, A.D. Pelton, P. Chartrand, C.D. Fuerst, Critical evaluation and thermodynamic optimization of the Al-Ce, Al-Y, Al-Sc and Mg-Sc binary systems, Calphad 32 (2008) 413–422.
[76] Y.-B. Kang, A.D. Pelton, P. Chartrand, P. Spencer, C.D. Fuerst, Critical evaluation and thermodynamic optimization of the binary systems in the Mg-Ce-Mn-Y system, J. Phase Equilib. Diffus. 28 (2007) 342–354.
[77] P. Ghosh, M. Mezbahul-Islam, M. Medraj, Critical assessment and thermodynamic modeling of Mg–Zn, Mg–Sn, Sn–Zn and Mg–Sn–Zn systems, Calphad 36 (2012) 28–43.
[78] P. Chartrand, A.D. Pelton, Thermodynamic evaluation and optimization of the LiCl-NaCl-KCl-RbCl-CsCl-$MgCl_2$-$CaCl_2$ system using the modified quasi-chemical model, Metall. Mater. Trans. A 32A (2001) 1361–1383.
[79] P. Chartrand, A.D. Pelton, Thermodynamic evaluation and optimization of the LiF-NaF-KF-MgF_2-CaF_2 system using the modified quasi-chemical model, Metall. Mater. Trans. A 32A (2001) 1385–1396.
[80] A.D. Pelton, A general "geometric" thermodynamic model for multicomponent solutions, Calphad 25 (2001) 319–328.
[81] Z.Y. Qiao, X. Xing, M. Peng, A. Mikula, Thermodynamic criterion for judging the symmetry of ternary systems and criterion applications, J. Phase. Equil. 17 (1996) 502–507.
[82] C. Bale, A. Pelton, W. Thompson, FactSage 6.4, Factsage thermochemical software and databases, http://www.crct.polymtl.ca/.
[83] K.C.H. Kumar, I. Ansara, P. Wollants, Sublattice modelling of the μ-phase, Calphad 22 (1998) 323–334.